CHAPTER 9
Phase Diagrams—Equilibrium Microstructural Development

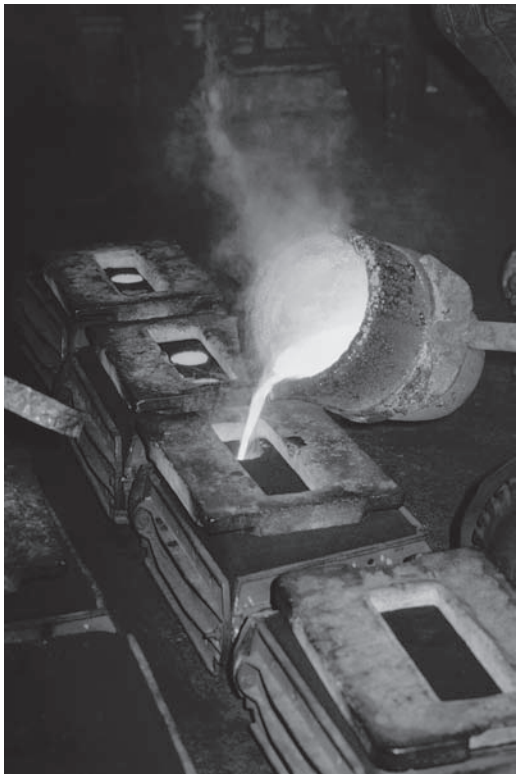

Phase diagrams can accurately predict the microstructures of metal alloys (like the brass shown here) if the casting is slowly cooled down to room temperature. (© Horizon International Images Limited / Alamy.)

From the beginning of this book we have seen that a fundamental concept of materials science is that the properties of materials follow from their atomic and microscopic structures. The dependence of transport and mechanical properties on atomic-scale structure was seen in Chapters 5 and 6. To appreciate fully the nature of the many microstructure-sensitive properties of engineering materials, we must spend some time exploring the ways in which microstructure is developed. An important tool in this exploration is the *phase diagram,* which is a map that will guide us in answering the general question: What microstructure should exist at a given temperature for a given material composition? This is a question with a specific answer based in part on the equilibrium nature of the material. Closely related is the next chapter, which deals with the heat treatment of materials. Still other related questions to be addressed in Chapter 10 will be "How fast will the microstructure form at a given temperature?" and "What temperature versus time history will result in an optimal microstructure?"

The discussion of microstructural development via phase diagrams begins with the *phase rule,* which identifies the number of microscopic phases associated with a given *state condition,* a set of values for temperature, pressure, and other variables that describe the nature of the material. We shall then describe the various characteristic phase diagrams for typical material systems. The *lever rule* will be used to quantify our interpretation of these phase diagrams. We shall specifically want to identify the composition and amount of each phase present. With these tools in hand, we can illustrate typical cases of microstructural development. Phase diagrams for several commercially important engineering materials are presented in this chapter. The most detailed discussion is reserved for the $Fe-Fe_3C$ diagram, which is the foundation for much of the iron and steel industry.

9.1 The Phase Rule

In this chapter we shall be quantifying the nature of microstructures. We begin with definitions of terms you need in order to understand the following discussion.

A **phase** is a chemically and structurally homogeneous portion of the microstructure. A single-phase microstructure can be polycrystalline (e.g., Figure 9.1), but each crystal grain differs only in crystalline orientation, not in chemical composition. Phase must be distinguished from **component**, which is a distinct chemical substance from which the phase is formed. For instance, we found in Section 4.1 that copper and nickel are so similar in nature that they are completely soluble in each other in any alloy proportions (e.g., Figure 4.2). For such a system, there is a single phase (a solid solution) and two components (Cu and Ni). For material systems involving compounds rather than elements, the compounds can be components. For example, MgO and NiO form solid solutions in a way similar to that for Cu and Ni (see Figure 4.5). In this case, the two components are MgO and NiO. As pointed out in Section 4.1, solid solubility is limited for many material systems. For certain compositions, the result is two phases, each richer in a different component. A classic example is the pearlite structure shown in Figure 9.2, which consists of alternating layers

FIGURE 9.1 *Single-phase microstructure of commercially pure molybdenum,* 200×. *Although there are many grains in this microstructure, each grain has the same uniform composition. (From* ASM Handbook, *Vol. 9:* Metallography and Microstructures, *ASM International, Materials Park, OH, 2004.)*

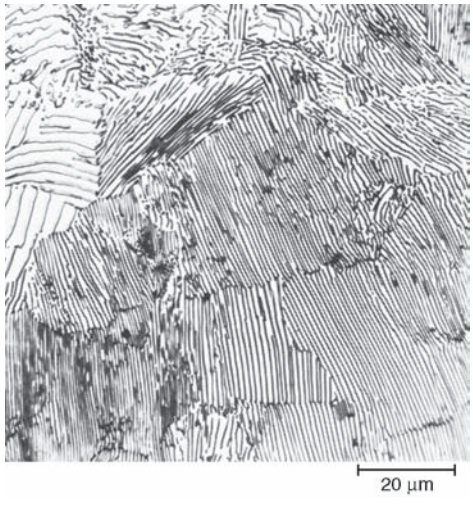

FIGURE 9.2 *Two-phase microstructure of pearlite found in a steel with* 0.8 *wt %* C, 650×. *This carbon content is an average of the carbon content in each of the alternating layers of ferrite (with* $<$ 0.02 *wt %* C) *and cementite (a compound,* Fe_3C, *which contains* 6.7 *wt %* C). *The narrower layers are the cementite phase. (From* ASM Handbook, *Vol. 9:* Metallography and Microstructures, *ASM International, Materials Park, OH, 2004.)*

of ferrite and cementite. The ferrite is α-Fe with a small amount of cementite in solid solution. The cementite is nearly pure Fe_3C. The components, then, are Fe and Fe_3C.

Describing the ferrite phase as α-Fe with cementite in solid solution is appropriate in terms of our definition of the components for this system. However, on the atomic scale, the solid solution consists of carbon atoms dissolved interstitially in the α-Fe crystal lattice. The component Fe_3C does not dissolve as a discrete molecular unit, which is generally true for compounds in solid solution.

A third term can be defined relative to *phase* and *component*. The **degrees of freedom** are the number of independent variables available to the system. For example, a pure metal at precisely its melting point has no degrees of freedom. At this condition, or **state**, the metal exists in two phases in equilibrium (i.e., in solid and liquid phases simultaneously). Any increase in temperature will change the state of the microstructure. (All of the solid phase will melt and become part of the liquid phase.) Similarly, even a slight reduction in temperature will completely solidify the material. The important **state variables** over which the materials engineer has control in establishing microstructure are temperature, pressure, and composition.

The general relationship between microstructure and these state variables is given by the **Gibbs*** **phase rule**, which, without derivation, can be stated as

$$F = C - P + 2, \tag{9.1}$$

where F is the number of degrees of freedom, C is the number of components, and P is the number of phases. The 2 in Equation 9.1 comes from limiting the state variables to two (temperature and pressure). For most routine materials processing involving condensed systems, the effect of pressure is slight, and we can consider pressure to be fixed at 1 atm. In this case, the phase rule can be rewritten to reflect one less degree of freedom:

$$F = C - P + 1. \tag{9.2}$$

For the case of the pure metal at its melting point, $C = 1$ and $P = 2$ (solid + liquid), giving $F = 1 - 2 + 1 = 0$, as we had noted previously. For a metal with a single impurity (i.e., with two components), solid and liquid phases can usually coexist over a range of temperatures (i.e., $F = 2 - 2 + 1 = 1$). The single degree of freedom means simply that we can maintain this two-phase microstructure while we vary the temperature of the material. However, we have only one independent variable ($F = 1$). By varying temperature, we indirectly vary the compositions of the individual phases. Composition is, then, a dependent variable. Such information that can be obtained from the Gibbs phase rule is most useful, but is also difficult to appreciate without the visual aid of phase diagrams. So, now we proceed to introduce these fundamentally important maps.

---

*Josiah Willard Gibbs (1839–1903), American physicist. As a professor of mathematical physics at Yale University, Gibbs was known as a quiet individual who made a profound contribution to modern science by almost singlehandedly developing the field of thermodynamics. His phase rule was a cornerstone of this achievement.

Our first example of a simple phase diagram is given in Figure 9.3. The one-component phase diagram [Figure 9.3(a)] summarizes the phases present for H_2O as a function of temperature and pressure. For the fixed pressure of 1 atm, we find a single, vertical temperature scale [Figure 9.3(b)] labeled with the appropriate transformation temperatures that summarize our common experience that solid H_2O (ice) transforms to liquid H_2O (water) at 0°C and that water transforms to gaseous H_2O (steam) at 100°C. More relevant to materials engineering, Figure 9.4 provides a similar illustration for pure iron. As practical engineering materials are typically impure, we shall next discuss phase diagrams, in the more general sense, for the case of more than one component.

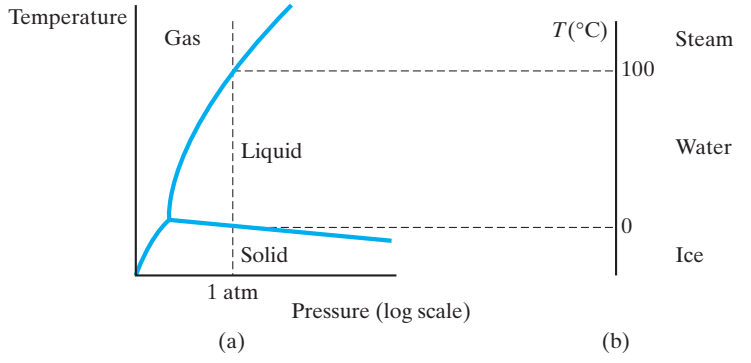

FIGURE 9.3 *(a) Schematic representation of the one-component phase diagram for* H_2O. *(b) A projection of the phase diagram information at 1 atm generates a temperature scale labeled with the familiar transformation temperatures for* H_2O *(melting at* 0°C *and boiling at* 100°C*).*

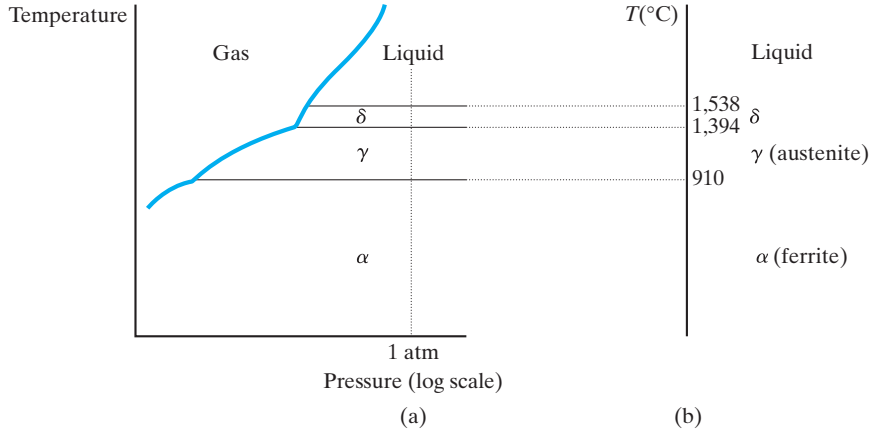

FIGURE 9.4 *(a) Schematic representation of the one-component phase diagram for pure iron. (b) A projection of the phase diagram information at 1 atm generates a temperature scale labeled with important transformation temperatures for iron. This projection will become one end of important binary diagrams, such as that shown in Figure 9.19.*

EXAMPLE 9.1

At 200°C, a 50:50 Pb–Sn solder alloy exists as two phases, a lead-rich solid and a tin-rich liquid. Calculate the degrees of freedom for this alloy and comment on its practical significance.

SOLUTION

Using Equation 9.2 (i.e., assuming a constant pressure of 1 atm above the alloy), we obtain

$$F = C - P + 1.$$

There are two components (Pb and Sn) and two phases (solid and liquid), giving

$$F = 2 - 2 + 1 = 1.$$

As a practical matter, we may retain this two-phase microstructure upon heating or cooling. However, such a temperature change exhausts the "freedom" of the system and must be accompanied by changes in composition. (The nature of the composition change will be illustrated by the Pb–Sn phase diagram shown in Figure 9.16.)

PRACTICE PROBLEM 9.1

Calculate the degrees of freedom at a constant pressure of 1 atm for **(a)** a single-phase solid solution of Sn dissolved in the solvent Pb, **(b)** pure Pb below its melting point, and **(c)** pure Pb at its melting point. (See Example 9.1.)

9.2 The Phase Diagram

A **phase diagram** is any graphical representation of the state variables associated with microstructures through the Gibbs phase rule. As a practical matter, phase diagrams in wide use by materials engineers are **binary diagrams**, which represent two-component systems ($C = 2$ in the Gibbs phase rule), and ternary diagrams, which represent three-component systems ($C = 3$). In this book, our discussion will be restricted to the binary diagrams. There are an abundant number of important binary systems that will give us full appreciation of the power of the phase rule, and at the same time, we avoid the complexities involved in extracting quantitative information from ternary diagrams.

In the following examples, keep in mind that phase diagrams are maps. Specifically, binary diagrams are maps of the equilibrium phases associated with various combinations of temperature and composition. Our concern will be to illustrate the change in phases and associated microstructure that follows from changes in the state variables (temperature and composition).

COMPLETE SOLID SOLUTION

Probably the simplest type of phase diagram is that associated with binary systems in which the two components exhibit **complete solid solution** in each other in both the solid and the liquid states. There have been previous references to such completely miscible behavior for Cu and Ni and for MgO and NiO. Figure 9.5 shows a typical phase diagram for such a system. Note that the diagram shows temperature as the variable on the vertical scale and composition as the horizontal variable. The melting points of pure components A and B are indicated. For relatively high temperatures, any composition will have melted completely to give a liquid **phase field**, the region of the phase diagram that corresponds to the existence of a liquid and that is labeled L. In other words, A and B are completely soluble in each other in the liquid state. What is unusual about this system is that A and B are also completely soluble in the solid state. The Hume-Rothery rules (see Section 4.1) state the criteria for this phenomenon in metal systems. In this book, we shall generally encounter complete miscibility in the liquid state (e.g., the L field in Figure 9.5). However, there are some systems in which liquid immiscibility occurs. Oil and water is a commonplace example. More relevant to materials engineering is the combination of various silicate liquids.

At relatively low temperatures, there is a single, solid-solution phase field labeled SS. Between the two single-phase fields is a two-phase region labeled L+SS. The upper boundary of the two-phase region is called the **liquidus** (i.e., the line above which a single liquid phase will be present). The lower boundary of the two-phase region is called the **solidus** and is the line below which the system has completely solidified. At a given **state point** (a pair of temperature and composition values) within the two-phase region, an A-rich liquid exists in equilibrium with a B-rich solid solution. The composition of each phase is established, as shown in Figure 9.6. The horizontal (constant-temperature) line passing through the state point cuts across both the liquidus and solidus lines. The composition

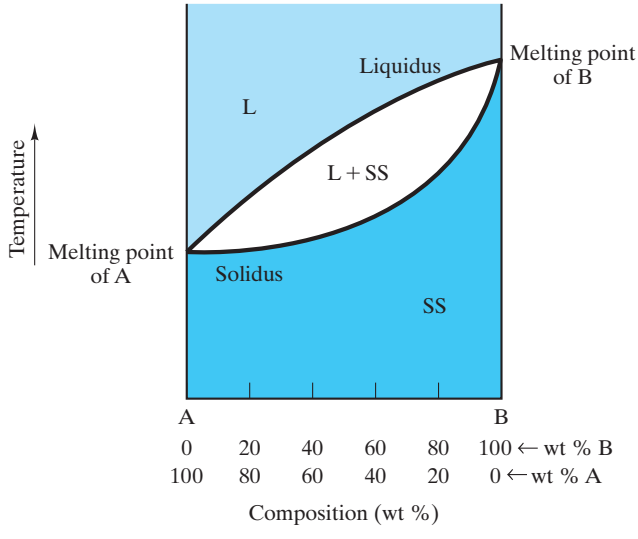

FIGURE 9.5 *Binary phase diagram showing complete solid solution. The liquid-phase field is labeled* L, *and the solid solution is designated* SS. *Note the two-phase region labeled* L + SS.

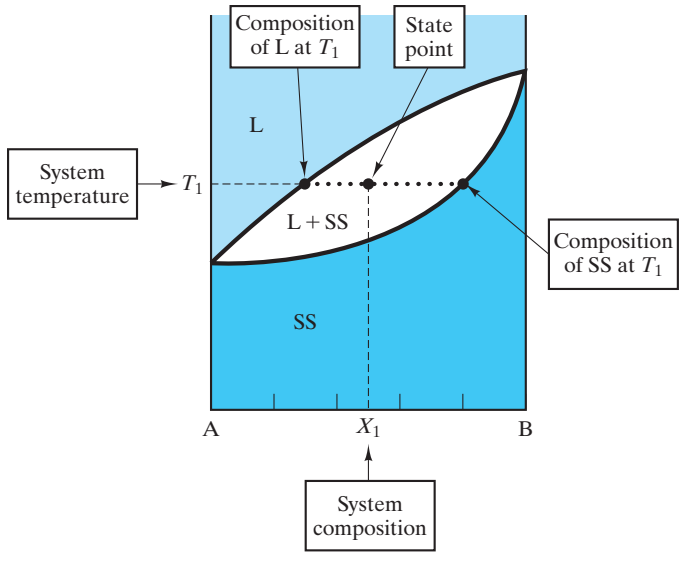

FIGURE 9.6 *The compositions of the phases in a two-phase region of the phase diagram are determined by a tie line (the horizontal line connecting the phase compositions at the system temperature).*

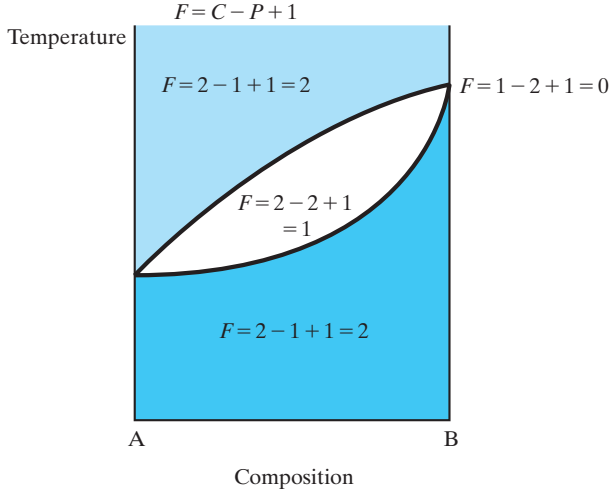

FIGURE 9.7 *Application of Gibbs phase rule (Equation 9.2) to various points in the phase diagram of Figure 9.5.*

of the liquid phase is given by the intersection point with the liquidus. Similarly, the solid solution composition is established by the point of intersection with the solidus. This horizontal line connecting the two phase compositions is termed a **tie line**. This construction will prove even more useful in Section 9.3 when we calculate the relative amounts of the two phases by the lever rule.

Figure 9.7 shows the application of the Gibbs phase rule (Equation 9.2) to various points in this phase diagram. The discussions in Section 9.1 can now be appreciated in terms of the graphical summary provided by the phase diagram. For example, an **invariant point** (where $F = 0$) occurs at the melting point of

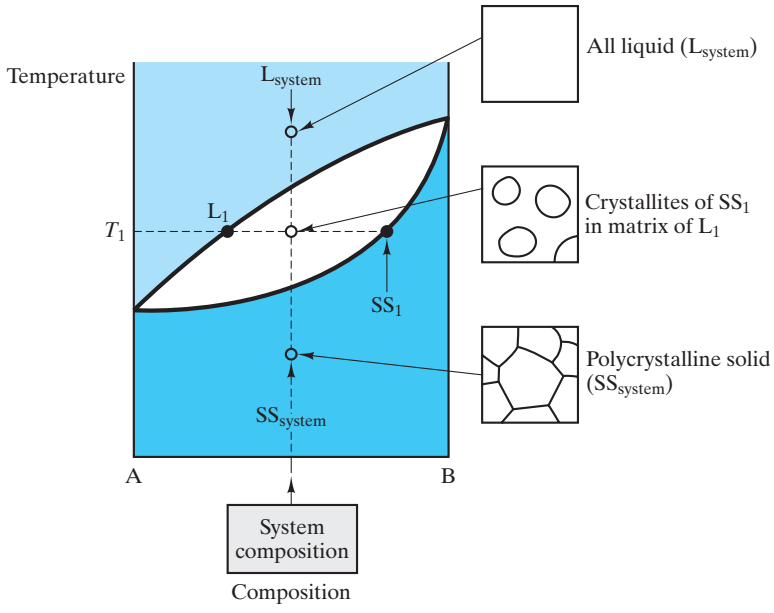

FIGURE 9.8 *Various microstructures characteristic of different regions in the complete solid-solution phase diagram.*

pure component B. At this limiting case, the material becomes a one-component system, and any change of temperature changes the microstructure to either all liquid (for heating) or all solid (for cooling). Within the two-phase (L + SS) region, there is one degree of freedom. A change of temperature is possible, but as Figure 9.6 indicates, the phase compositions are not independent. Instead, they will be established by the tie line associated with a given temperature. In the single-phase solid-solution region, there are two degrees of freedom; that is, both temperature and composition can be varied independently without changing the basic nature of the microstructure. Figure 9.8 summarizes microstructures characteristic of the various regions of this phase diagram.

By far the greatest use of phase diagrams in materials engineering is for the inorganic materials of importance to the metals and ceramics industries. Polymer applications generally involve single-component systems and/or nonequilibrium structures that are not amenable to presentation as phase diagrams. The common use of high-purity phases in the semiconductor industry also makes phase diagrams of limited use. The Cu–Ni system in Figure 9.9 is the classic example of a binary diagram with complete solid solution. A variety of commercial copper and nickel alloys falls within this system, including a superalloy called Monel.

The NiO–MgO system (Figure 9.10) is a ceramic system analogous to the Cu–Ni system (i.e., exhibiting complete solid solution). While the Hume-Rothery rules (Section 4.1) addressed solid solution in metals, the requirement of similarity of cations is a comparable basis for solid solution in this oxide structure (see Figure 4.5).

Note that the composition axis for the NiO–MgO phase diagram (and the other ceramic phase diagrams) is expressed in mole percent rather than weight percent. The use of mole percent has no effect on the validity of the lever-rule calculations that we will make in Section 9.3. The only effect on the results is that

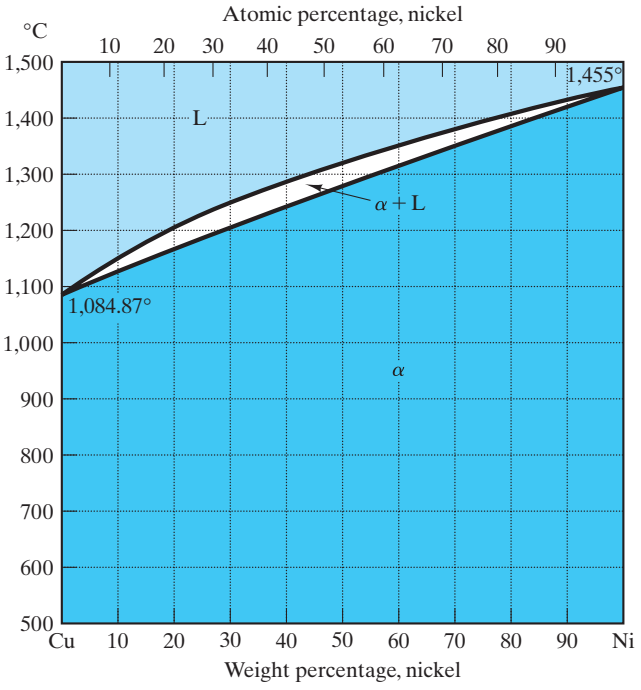

FIGURE 9.9 Cu–Ni *phase diagram. (From* Metals Handbook, *8th ed., Vol. 8:* Metallography, Structures, and Phase Diagrams, *American Society for Metals, Metals Park, OH, 1973, and* Binary Alloy Phase Diagrams, *Vol. 1, T. B. Massalski, Ed., American Society for Metals, Metals Park, OH, 1986.)*

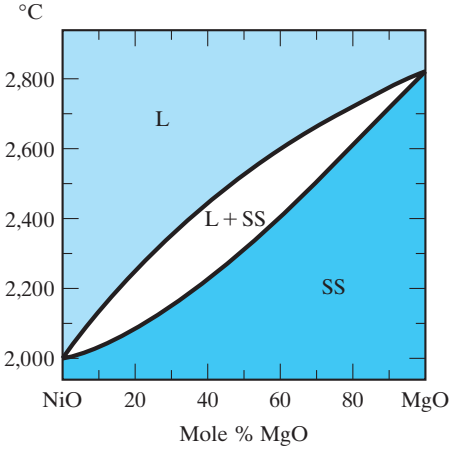

FIGURE 9.10 NiO–MgO *phase diagram. (After* Phase Diagrams for Ceramists, *Vol. 1, American Ceramic Society, Columbus, OH, 1964.) (Reprinted with permission of The American Ceramic Society (www.ceramics.org). All rights reserved.)*

the answers obtained from such a calculation are in mole fractions rather than weight fractions.

EUTECTIC DIAGRAM WITH NO SOLID SOLUTION

We now turn to a binary system that is the opposite of the one just discussed. Some components are so dissimilar that their solubility in each other is nearly negligible. Figure 9.11 illustrates the characteristic phase diagram for such a

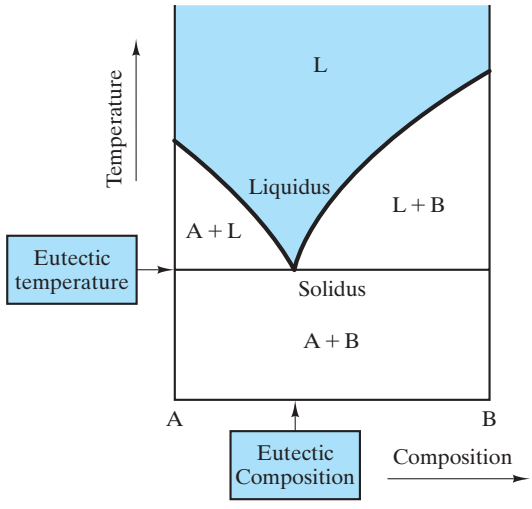

FIGURE 9.11 *Binary eutectic phase diagram showing no solid solution. This general appearance can be contrasted to the opposite case of complete solid solution illustrated in Figure 9.5.*

system. Several features distinguish this diagram from the type characteristic of complete solid solubility. First is the fact that, at relatively low temperatures, there is a two-phase field for pure solids A and B, consistent with our observation that the two components (A and B) cannot dissolve in each other. Second, the solidus is a horizontal line that corresponds to the **eutectic temperature**. This name comes from the Greek word *eutektos,* meaning "easily melted." In this case, the material with the **eutectic composition** is fully melted at the eutectic temperature. Any composition other than the eutectic will not fully melt at the eutectic temperature. Instead, such a material must be heated further through a two-phase region to the liquidus line. This situation is analogous to the two-phase region (L + SS) found in Figure 9.5. Figure 9.11 differs in that we have two such two-phase regions (A + L and B + L) in the binary eutectic diagram.

Some representative microstructures for the binary **eutectic diagram** are shown in Figure 9.12. The liquid and the liquid + solid microstructures are comparable to cases found in Figure 9.8. However, a fundamental difference exists in the microstructure of the fully solid system. In Figure 9.12, we find a fine-grained eutectic microstructure in which there are alternating layers of the components, pure A and pure B. A fuller discussion of solid-state microstructures will be appropriate after the lever rule has been introduced in Section 9.3. For now, we can emphasize that the sharp solidification point of the eutectic composition generally leads to the fine-grained nature of the eutectic microstructure. Even during slow cooling of the eutectic composition through the eutectic temperature, the system must transform from the liquid state to the solid state relatively quickly. The limited time available prevents a significant amount of diffusion (Section 5.3). The segregation of A and B atoms (which were randomly mixed in the liquid state) into separate solid phases must be done on a small scale. Various morphologies occur for various eutectic systems. But whether lamellar, nodular, or other morphologies are stable, these various eutectic microstructures are commonly fine-grained.

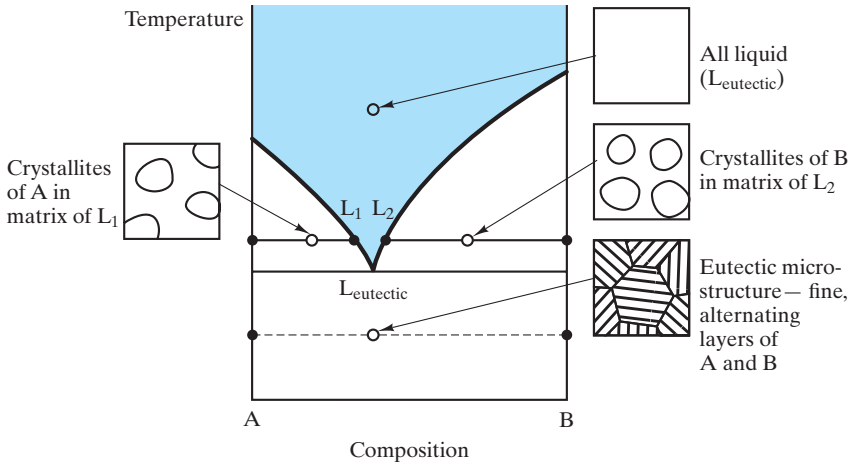

FIGURE 9.12 *Various microstructures characteristic of different regions in a binary eutectic phase diagram with no solid solution.*

The simple eutectic system Al–Si (Figure 9.13) is a close approximation to Figure 9.11, although a small amount of solid solubility does exist. The aluminum-rich side of the diagram describes the behavior of some important aluminum alloys. Although we are not dwelling on semiconductor-related examples, the silicon-rich side illustrates the limit of aluminum doping in producing *p*-type semiconductors (see Chapter 13).

EUTECTIC DIAGRAM WITH LIMITED SOLID SOLUTION

For many binary systems, the two components are partially soluble in each other. The result is a phase diagram intermediate between the two cases we have treated so far. Figure 9.14 shows a eutectic diagram with limited solid solution. It generally looks like Figure 9.11 except for the solid-solution regions near each edge. These single-phase regions are comparable to the SS region in Figure 9.5 except for the fact that the components in Figure 9.14 do not exist in a single solid solution near the middle of the composition range. As a result, the two solid-solution phases, α and β, are distinguishable, and they frequently have different crystal structures. In any case, the crystal structure of α will be that of A, and the crystal structure of β will be that of B because each component serves as a solvent for the other, "impurity" component (e.g., α consists of B atoms in solid solution in the crystal lattice of A). The use of tie lines to determine the compositions of α and β in the two-phase regions is identical to the diagram shown in Figure 9.6, and examples are shown in Figure 9.15 together with representative microstructures.

The Pb–Sn system (Figure 9.16) is a good example of a binary eutectic with limited solid solution. Common solder alloys fall within this system. Their low melting ranges allow for joining of most metals by convenient heating methods, with low risk of damage to heat-sensitive parts. Solders with less than 5 wt % tin are used for sealing containers and coating and joining metals, and are also used for applications with service temperatures that exceed 120°C. Solders with between 10 and 20 wt % tin are used for sealing cellular automobile radiators

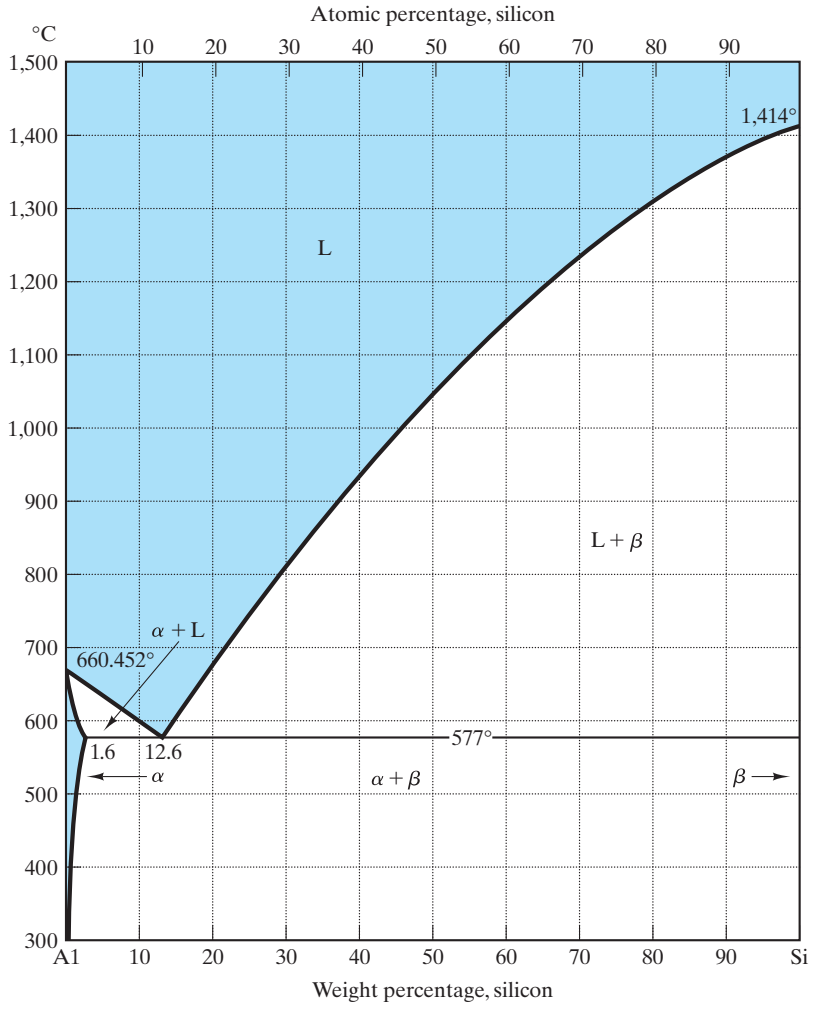

FIGURE 9.13 Al–Si *phase diagram. (After* Binary Alloy Phase Diagrams, *Vol. 1, T. B. Massalski, Ed., American Society for Metals, Metals Park, OH, 1986.)*

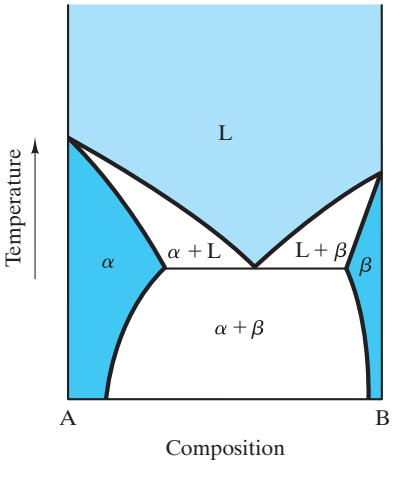

FIGURE 9.14 *Binary eutectic phase diagram with limited solid solution. The only difference between this diagram and the one shown in Figure 9.11 is the presence of solid-solution regions α and β.*

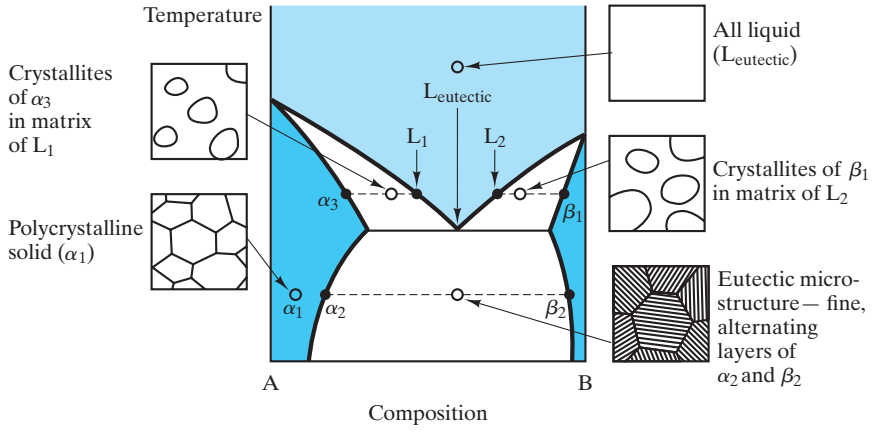

FIGURE 9.15 *Various microstructures characteristic of different regions in the binary eutectic phase diagram with limited solid solution. This illustration is essentially equivalent to the illustration shown in Figure 9.12, except that the solid phases are now solid solutions* (α *and* β) *rather than pure components* (A *and* B).

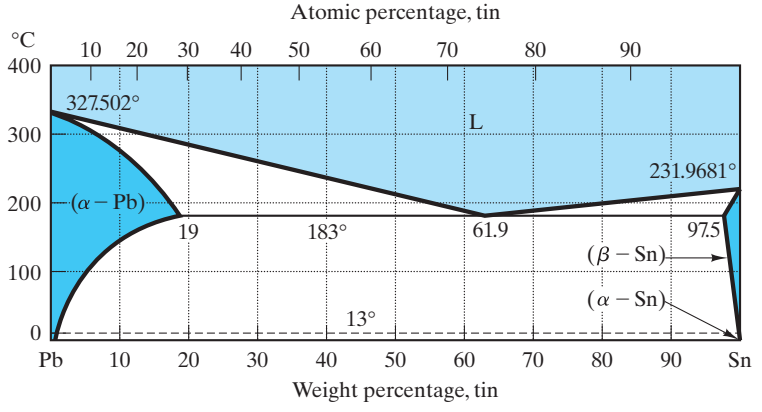

FIGURE 9.16 Pb–Sn *phase diagram. (After* Metals Handbook, *8th ed., Vol. 8:* Metallography, Structures, and Phase Diagrams, *American Society for Metals, Metals Park, Ohio, 1973, and* Binary Alloy Phase Diagrams, *Vol. 2, T. B. Massalski, Ed., American Society for Metals, Metals Park, OH, 1986.)*

and filling seams and dents in automobile bodies. General-purpose solders are generally 40 or wt % tin. These solders have a characteristic pastelike consistency during application, associated with the two-phase liquid plus solid region just above the eutectic temperature. Their wide range of applications includes well-known examples from plumbing to electronics. Solders near the eutectic composition (approximately 60 wt % tin) are used for heat-sensitive electronic components that require minimum heat application. It should be noted that, when we arrive at the end of this book (Section 15.4 dealing with materials and our environment), some of these useful applications of lead solders are being constrained by environmental policy due to the toxicity of lead.

EUTECTOID DIAGRAM

The transformation of eutectic liquid to a relatively fine-grained microstructure of two solid phases upon cooling can be described as a special type of chemical reaction. This **eutectic reaction** can be written as

$$\text{L (eutectic)} \xrightarrow{\text{cooling}} \alpha + \beta, \tag{9.3}$$

where the notation corresponds to the phase labels from Figure 9.14. Some binary systems contain a solid-state analog of the eutectic reaction. Figure 9.17 illustrates such a case. The *eutectoid reaction* is

$$\gamma\text{(eutectoid)} \xrightarrow{\text{cooling}} \alpha + \beta, \tag{9.4}$$

where *eutectoid* means "eutectic-like." Some representative microstructures are shown in the **eutectoid diagram** of Figure 9.18. The different morphologies of the eutectic and eutectoid microstructures emphasize our previous point that although the specific nature of these diffusion-limited structures will vary, they will generally be relatively fine grained. A eutectoid reaction plays a fundamental role in the technology of steelmaking.

The $Fe-Fe_3C$ system (Figure 9.19) is, by far, the most important commercial phase diagram we shall encounter. It provides the major scientific basis for the iron and steel industries. In Chapter 11, the boundary between irons and steels will be identified as a carbon content of 2.0 wt %. This point roughly corresponds to the carbon solubility limit in the **austenite*** (γ) phase of Figure 9.19.

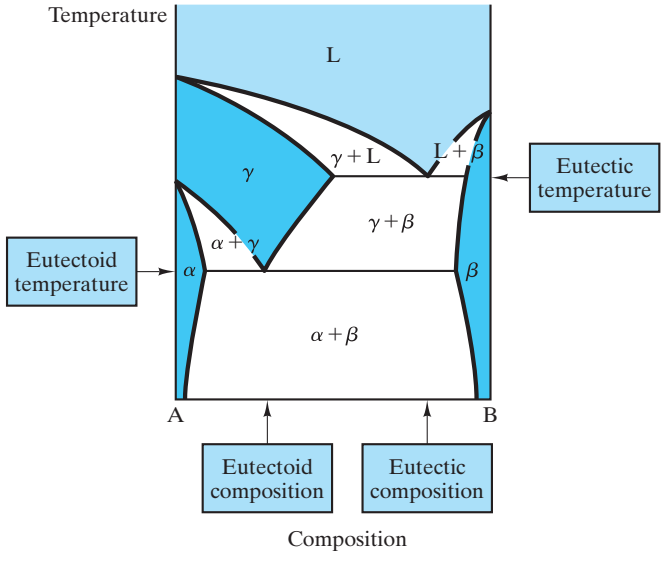

FIGURE 9.17 *This eutectoid phase diagram contains both a eutectic reaction (Equation 9.3) and its solid-state analog, a eutectoid reaction (Equation 9.4).*

*William Chandler Roberts-Austen (1843–1902), English metallurgist. Young William Roberts set out to be a mining engineer, but his opportunities led to an appointment in 1882 as "chemist and assayer of the mint," a position he held until his death. His varied studies of the technology of coin making led to his appointment as a professor of metallurgy at the Royal School of Mines. He was a great success in both his government and academic posts. His textbook, *Introduction to the Study of Metallurgy*, was published in six editions between 1891 and 1908. In 1885, he adopted the additional surname in honor of his uncle (Nathaniel Austen).

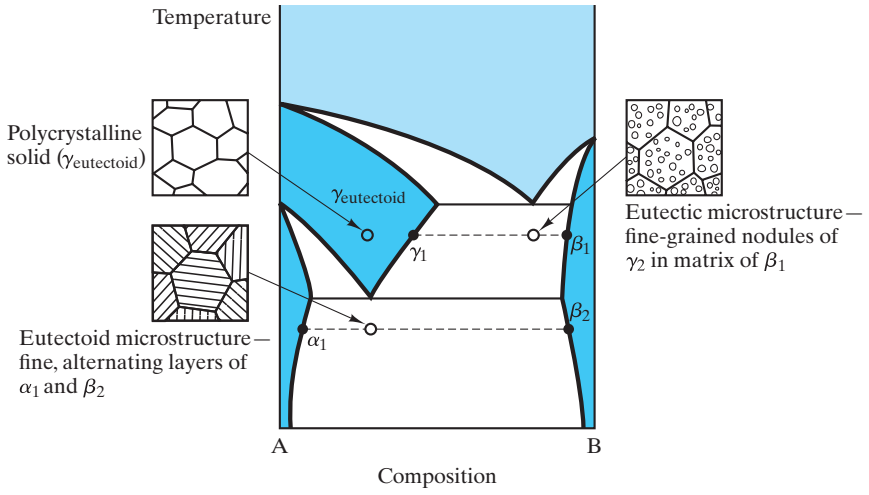

FIGURE 9.18 *Representative microstructures for the eutectoid diagram of Figure 9.17.*

POWERS OF 10

Micrometer scale structures such as these developed during the slow cooling of commercial alloys play a central role in contemporary industries. Among the most important examples are Figures 9.19 and 9.20 relative to the iron and steel industries. More detailed examples are illustrated in Section 9.4.

In addition, this diagram is representative of microstructural development in many related systems with three or more components (e.g., some stainless steels that include large amounts of chromium). Although Fe_3C, and not carbon, is a component in this system, the composition axis is customarily given in weight percent carbon. The important areas of interest on this diagram are around the eutectic and the eutectoid reactions. The reaction near 1,500°C is of no practical consequence.

A final note of some irony is that the Fe–Fe_3C diagram is not a true equilibrium diagram. The Fe–C system (Figure 9.20) represents true equilibrium. Although graphite (C) is a more stable precipitate than Fe_3C, the rate of graphite precipitation is enormously slower than that of Fe_3C. The result is that in common steels (and many cast irons) the Fe_3C phase is **metastable**; that is, for all practical purposes it is stable with time and conforms to the Gibbs phase rule.

As just noted, the Fe–C system (Figure 9.20) is fundamentally more stable, but less common than the Fe–Fe_3C system because of slow *kinetics* (the subject of Chapter 10). Extremely slow cooling rates can produce the results indicated on the Fe–C diagram. The more practical method is to promote graphite precipitation by a small addition of a third component, such as silicon. Typically, silicon additions of 2 to 3 wt % are used to stabilize the graphite precipitation. This third component is not acknowledged in Figure 9.20. The result, however, is that the figure does describe microstructural development for some practical systems. An example will be given in Section 9.4.

PERITECTIC DIAGRAM

In all the binary diagrams inspected to this point, the pure components have had distinct melting points. In some systems, however, the components will form stable compounds that may not have such a distinct melting point. An example is illustrated in Figure 9.21. In this simple example, A and B form the stable compound AB, which does not melt at a single temperature as do components A and B. An additional simplification used here is to ignore the possibility of some

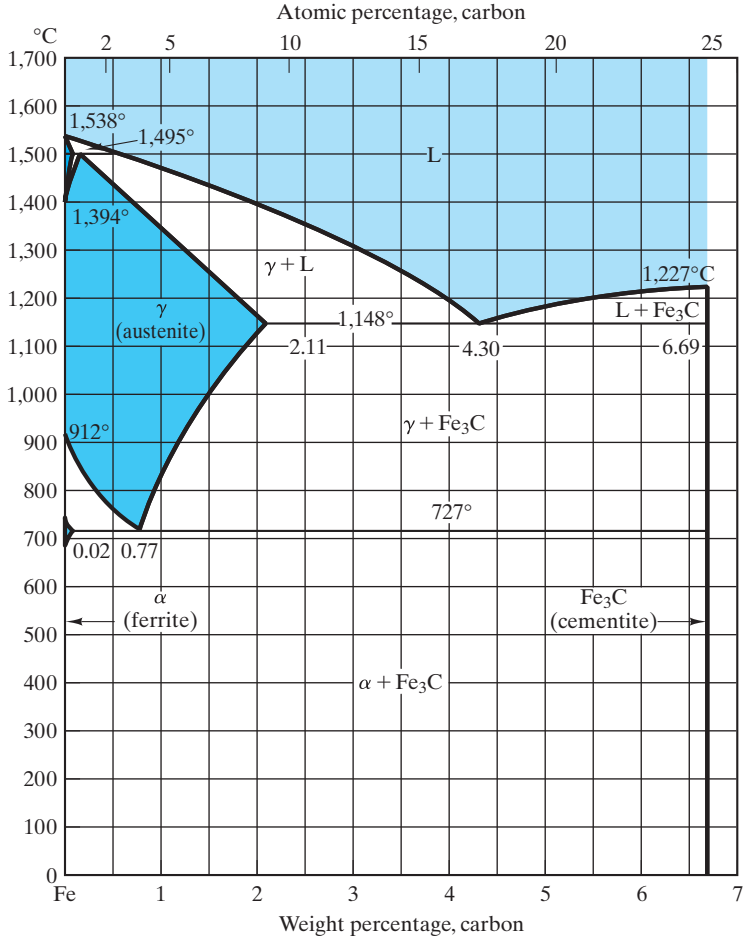

FIGURE 9.19 Fe–Fe_3C *phase diagram. Note that the composition axis is given in weight percent carbon even though* Fe_3C*, and not carbon, is a component. (After* Metals Handbook*, 8th ed., Vol. 8:* Metallography, Structures, and Phase Diagrams*, American Society for Metals, Metals Park, OH, 1973, and* Binary Alloy Phase Diagrams*, Vol. 1, T. B. Massalski, Ed., American Society for Metals, Metals Park, OH, 1986.)*

solid solution for the components and intermediate compound. The components are said to undergo **congruent melting**; that is, the liquid formed upon melting has the same composition as the solid from which it was formed. On the other hand, compound AB (which is 50 mol % A plus 50 mol % B) is said to undergo **incongruent melting**; that is, the liquid formed upon melting has a composition other than AB. The term *peritectic* is used to describe this incongruent melting phenomenon. *Peritectic* comes from the Greek phrase meaning to "melt nearby." The **peritectic reaction** can be written as

$$\text{AB} \xrightarrow{\text{heating}} \text{L} + \text{B}, \tag{9.5}$$

where the liquid composition is noted in the **peritectic diagram** of Figure 9.21. Some representative microstructures are shown in Figure 9.22. The Al_2O_3–SiO_2 phase diagram (Figure 9.23) is a classic example of a peritectic diagram.

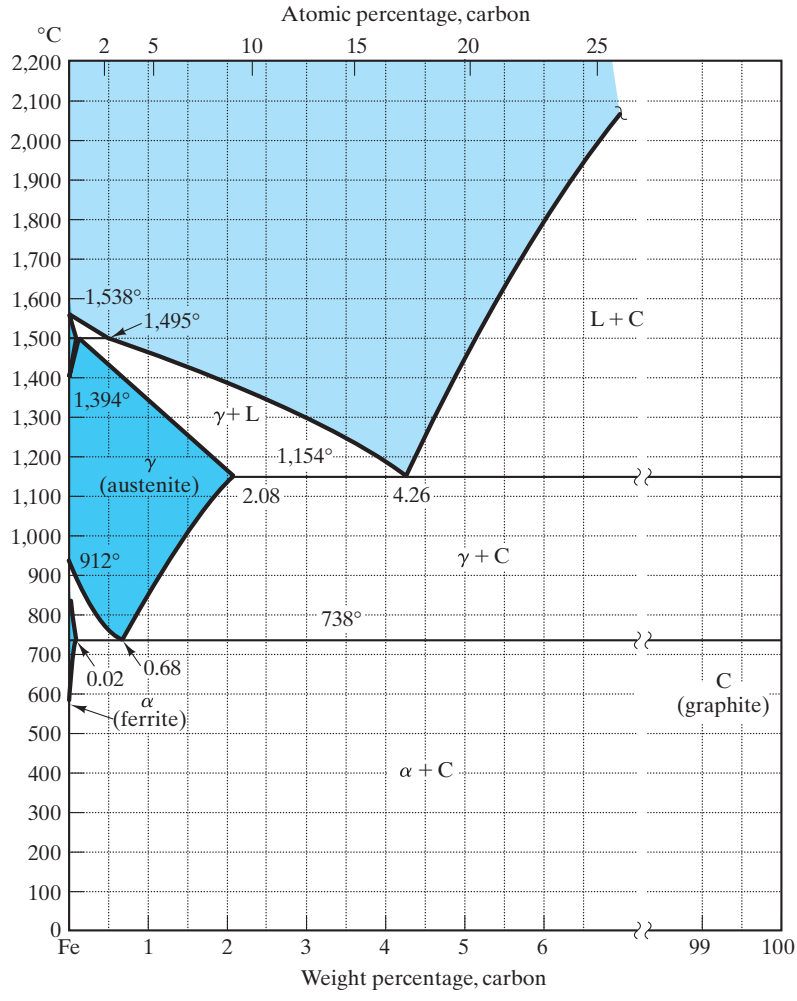

FIGURE 9.20 Fe–C *phase diagram. The left side of this diagram is nearly identical to the left side of the* Fe–Fe_3C *diagram (Figure 9.19). In this case, however, the intermediate compound* Fe_3C *does not exist. (After* Metals Handbook, *8th ed., Vol. 8:* Metallography, Structures, and Phase Diagrams, *American Society for Metals, Metals Park, OH, 1973, and* Binary Alloy Phase Diagrams, *Vol. 1, T. B. Massalski, Ed., American Society for Metals, Metals Park, OH, 1986.)*

The Al_2O_3–SiO_2 binary diagram is as important to the ceramic industry as the Fe–Fe_3C diagram is to the steel industry. Several important ceramics fall within this system. Refractory silica bricks are nearly pure SiO_2, with 0.2 to 1.0 wt % (0.1 to 0.6 mol %) Al_2O_3. For silica bricks required to operate at temperatures above 1,600°C, it is obviously important to keep the Al_2O_3 content as low as possible (by careful raw material selection) to minimize the amount of liquid phase. A small amount of liquid is tolerable. Common fireclay refractories are located in the range of 25 to 45 wt % (16 to 32 mol %) Al_2O_3. Their utility as structural elements in furnace designs is limited by the solidus (eutectic) temperature of 1,587°C. A dramatic increase in *refractoriness,* or temperature resistance, occurs at the composition of the incongruently melting compound mullite ($3Al_2O_3 \cdot 2SiO_2$).

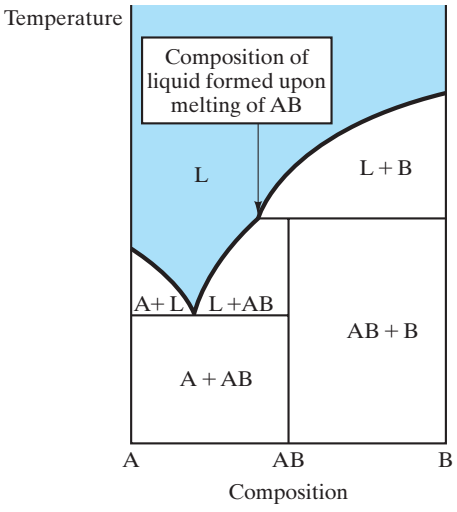

FIGURE 9.21 *Peritectic phase diagram showing a peritectic reaction (Equation 9.5). For simplicity, no solid solution is shown.*

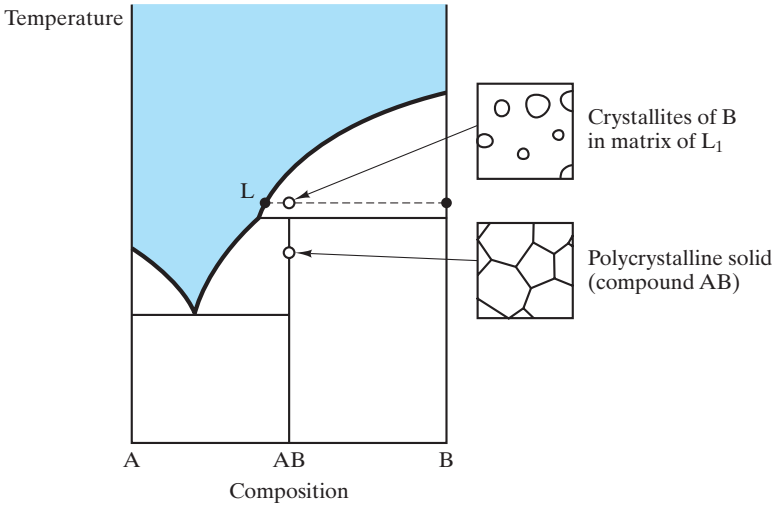

FIGURE 9.22 *Representative microstructures for the peritectic diagram of Figure 9.21.*

A controversy over the nature of the melting for mullite has continued for several decades. The peritectic reaction shown in Figure 9.23 is now widely accepted. The debate about such a commercially important system illustrates a significant point. Establishing equilibrium in high-temperature ceramic systems is not easy. Silicate glasses are similar examples of this point. Phase diagrams for this text represent our best understanding at this time, but we must remain open to refined experimental results in the future.

Care is exercised in producing mullite refractories to ensure that the overall composition is greater than 72 wt % (60 mol %) Al_2O_3 to avoid the two-phase region (mullite + liquid). By so doing, the refractory remains completely solid to the peritectic temperature of 1,890°C. So-called high-alumina refractories fall within the composition range 60 to 90 wt % (46 to 84 mol %) Al_2O_3. Nearly pure

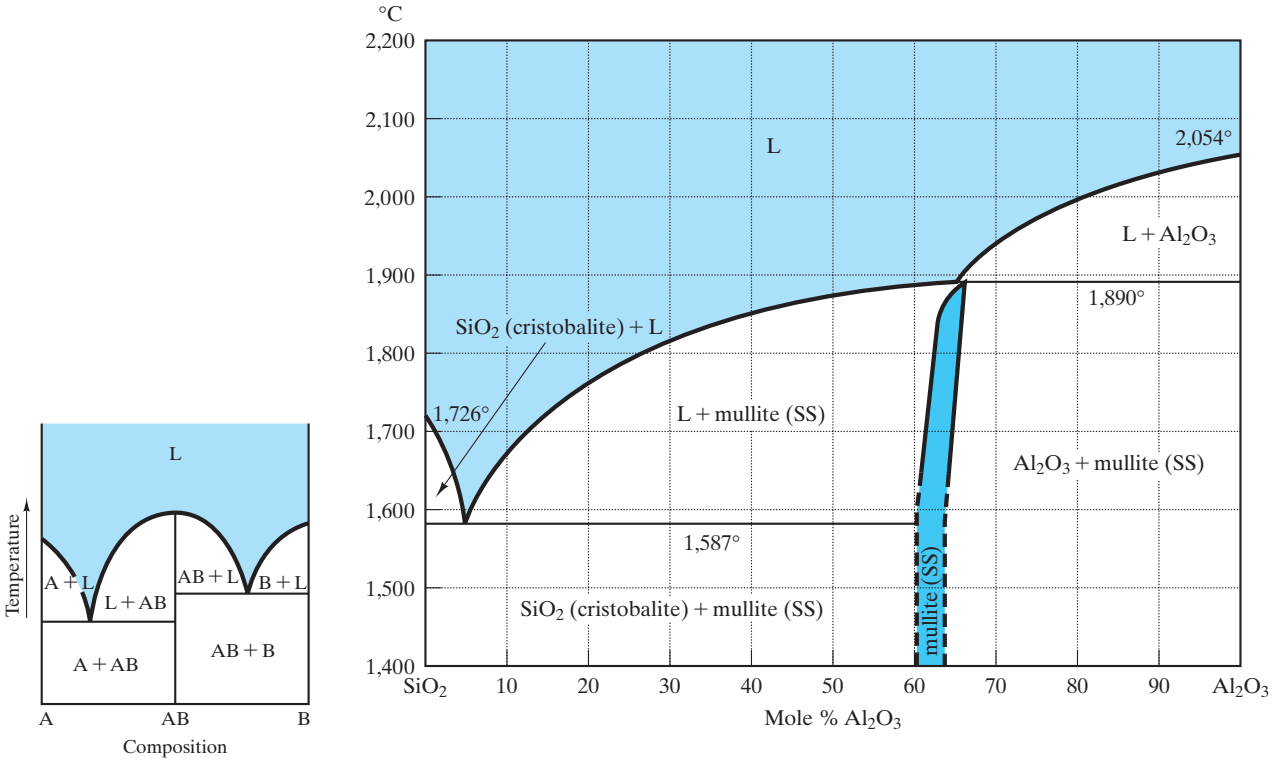

FIGURE 9.23 Al_2O_3–SiO_2 *phase diagram. Mullite is an intermediate compound with ideal stoichiometry* $3Al_2O_3 \cdot 2SiO_2$. *(After F. J. Klug, S. Prochazka, and R. H. Doremus,* J. Am. Ceram. Soc. 70*, 750, 1987.) (Reprinted with permission of The American Ceramic Society (www.ceramics.org). All rights reserved.)*

Al_2O_3 represents the highest refractoriness (temperature resistance) of commercial materials in the Al_2O_3–SiO_2 system. These materials are used in such demanding applications as refractories in glass manufacturing and laboratory crucibles.

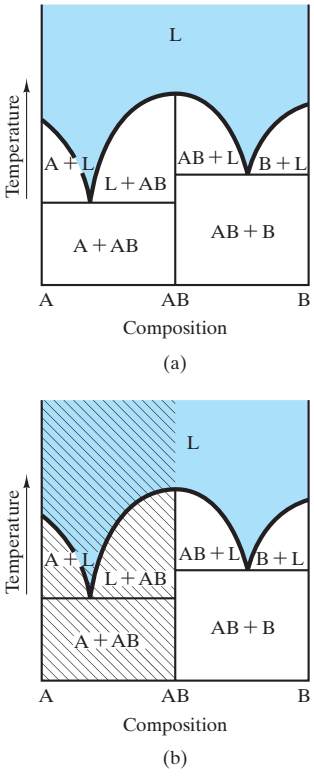

FIGURE 9.24 *(a) Binary phase diagram with a congruently melting intermediate compound,* AB. *This diagram is equivalent to two simple binary eutectic diagrams (the* A–AB *and* AB–B *systems). (b) For analysis of microstructure for an overall composition in the* AB–B *system, only that binary eutectic diagram need be considered.*

GENERAL BINARY DIAGRAMS

The peritectic diagram was our first example of a binary system with an **intermediate compound**, a chemical compound formed between two components in a binary system. In fact, the formation of intermediate compounds is a relatively common occurrence. Of course, such compounds are not associated solely with the peritectic reaction. Figure 9.24(a) shows the case of an intermediate compound, AB, which melts congruently. An important point about this system is that it is equivalent to two adjacent binary eutectic diagrams of the type first introduced in Figure 9.11. Again, for simplicity, we are ignoring solid solubility. This is our first encounter with what can be termed a **general diagram**, a composite of two or more of the types covered in this section. The approach to analyzing these more complex systems is straightforward: Simply deal with the smallest binary system associated with the overall composition and ignore all others. This procedure is illustrated in Figure 9.24(b), which shows that for an overall composition between AB and B, we can treat the diagram as a simple binary eutectic of AB and B. For all practical purposes, the A–AB binary does not exist for

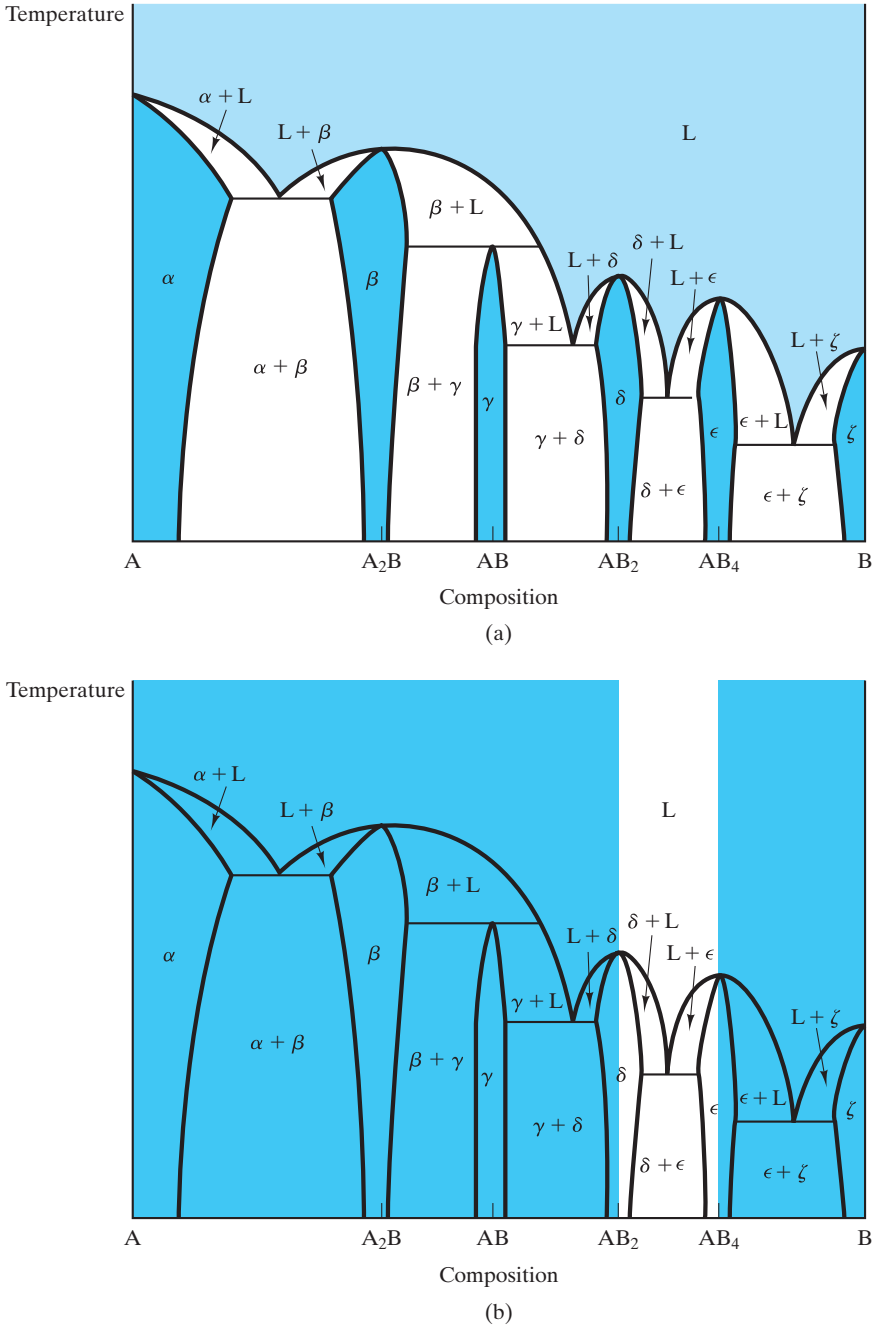

FIGURE 9.25 *(a) A relatively complex binary phase diagram. (b) For an overall composition between* AB_2 and AB_4*, only that binary eutectic diagram is needed to analyze microstructure.*

the overall composition shown in Figure 9.24(b). Nowhere in the development of microstructure for that composition will crystals of A be found in a liquid matrix or will crystals of A and AB exist simultaneously in equilibrium. A more elaborate illustration of this point is shown in Figure 9.25. In Figure 9.25(a), we

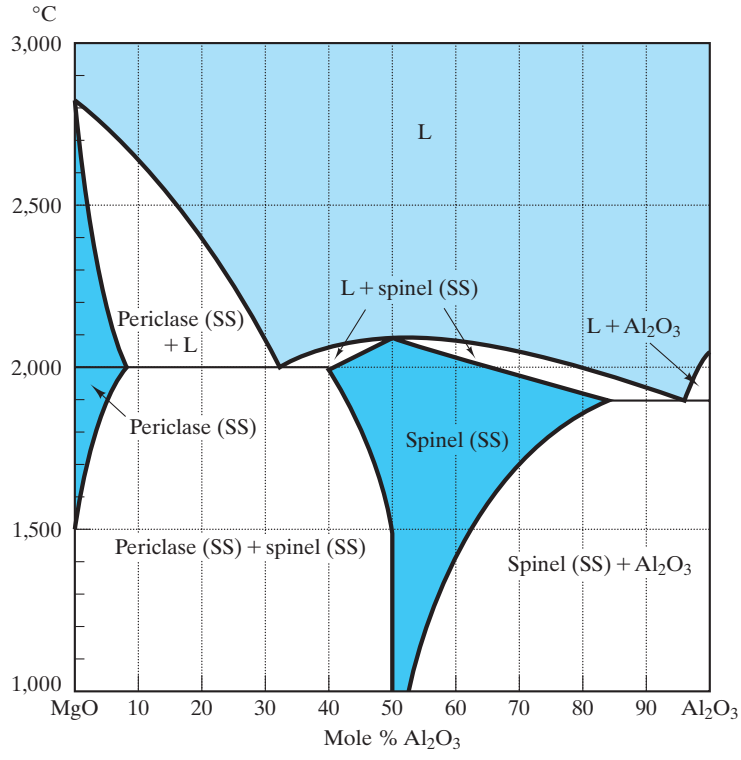

FIGURE 9.26 $MgO–Al_2O_3$ *phase diagram. Spinel is an intermediate compound with ideal stoichiometry* $MgO \cdot Al_2O_3$. *(After* Phase Diagrams for Ceramists, *Vol. 1, American Ceramic Society, Columbus, OH, 1964.) (Reprinted with permission of The American Ceramic Society (www.ceramics.org). All rights reserved.)*

find a relatively complex general diagram with four intermediate compounds (A_2B, AB, AB_2, and AB_4) and several examples of individual binary diagrams. But for the overall compositions shown in Figure 9.25(b), only the $AB_2–AB_4$ binary is relevant.

The $MgO–Al_2O_3$ system (Figure 9.26) is similar to that shown in Figure 9.24, but with limited solid solubility. Figure 9.26 includes the important intermediate compound, spinel, $MgO \cdot Al_2O_3$ or $MgAl_2O_4$, with an extensive solid-solution range. (A dilute solution of Al_2O_3 in MgO was illustrated in Figure 4.6.) Spinel refractories are widely used in industry. An important family of magnetic materials is based on the chemistry and crystal structure of spinel (see Chapter 14).

Figures 9.27 and 9.28 are good examples of general diagrams comparable to that shown in Figure 9.25. Important age-hardenable aluminum alloys are found near the κ phase boundary in the Al–Cu system (Figure 9.27).We will discuss this point in relation to Figure 9.36, and we will discuss the subtleties of precipitation hardening further in Section 10.4. The Al–Cu system is a good example of a complex diagram that can be analyzed as a simple binary eutectic in the high-aluminum region.

Like the Al–Cu system, the Cu–Zn system in Figure 9.28 is a complex diagram that is, for some practical systems, easy to analyze. For example, many commercial brass compositions lie in the single-phase α region.

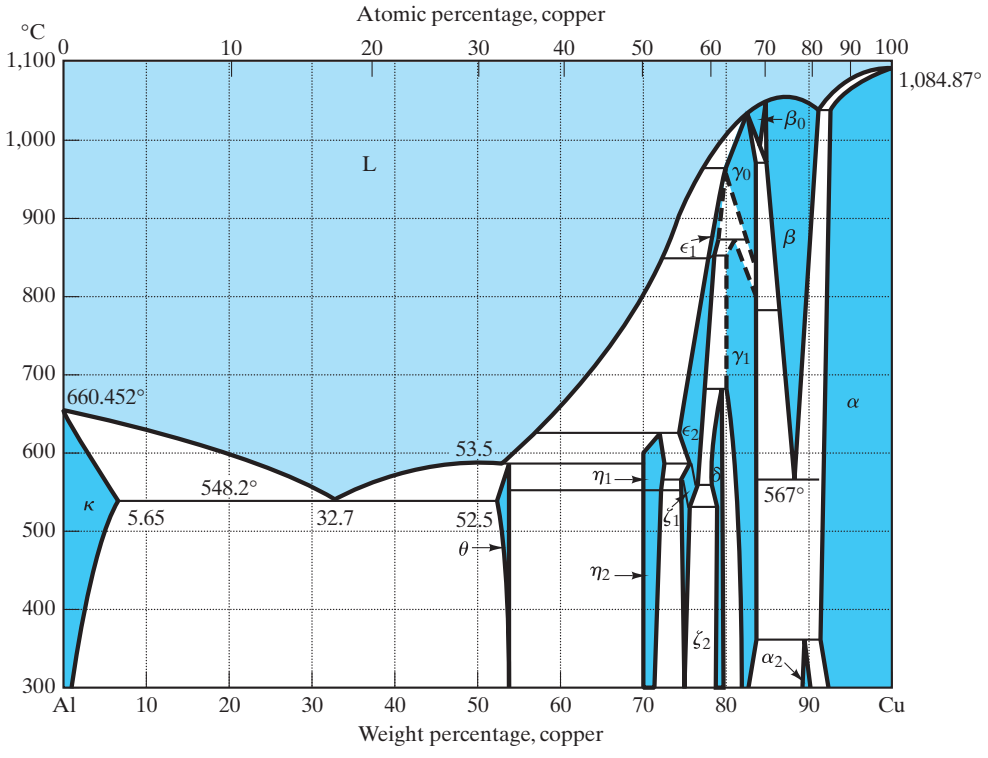

FIGURE 9.27 Al–Cu *phase diagram. (After* Binary Alloy Phase Diagrams*, Vol. 1, T. B. Massalski, Ed., American Society for Metals, Metals Park, OH, 1986.)*

The $CaO-ZrO_2$ phase diagram (Figure 9.29) is an example of a general diagram of a ceramic system. ZrO_2 has become an important refractory material through the use of stabilizing additions such as CaO. As seen in the phase diagram (Figure 9.29), pure ZrO_2 has a phase transformation at 1,000°C in which the crystal structure changes from monoclinic to tetragonal upon heating. This transformation involves a substantial volume change that is structurally catastrophic to the brittle ceramic. Cycling the pure material through the transformation temperature will effectively reduce it to powder. As the phase diagram also shows, the addition of approximately 10 wt % (20 mol %) CaO produces a solid-solution phase with a cubic crystal structure from room temperature to the melting point (near 2,500°C). This "stabilized zirconia" is a practical, and obviously very refractory, structural material. Various other ceramic components, such as Y_2O_3, serve as stabilizing components and have phase diagrams with ZrO_2 that look quite similar to the diagram shown in Figure 9.29.

EXAMPLE 9.2

An alloy in the A–B system described by Figure 9.25 is formed by melting equal parts of A and A_2B. Qualitatively describe the microstructural development that will occur upon slow cooling of this melt.

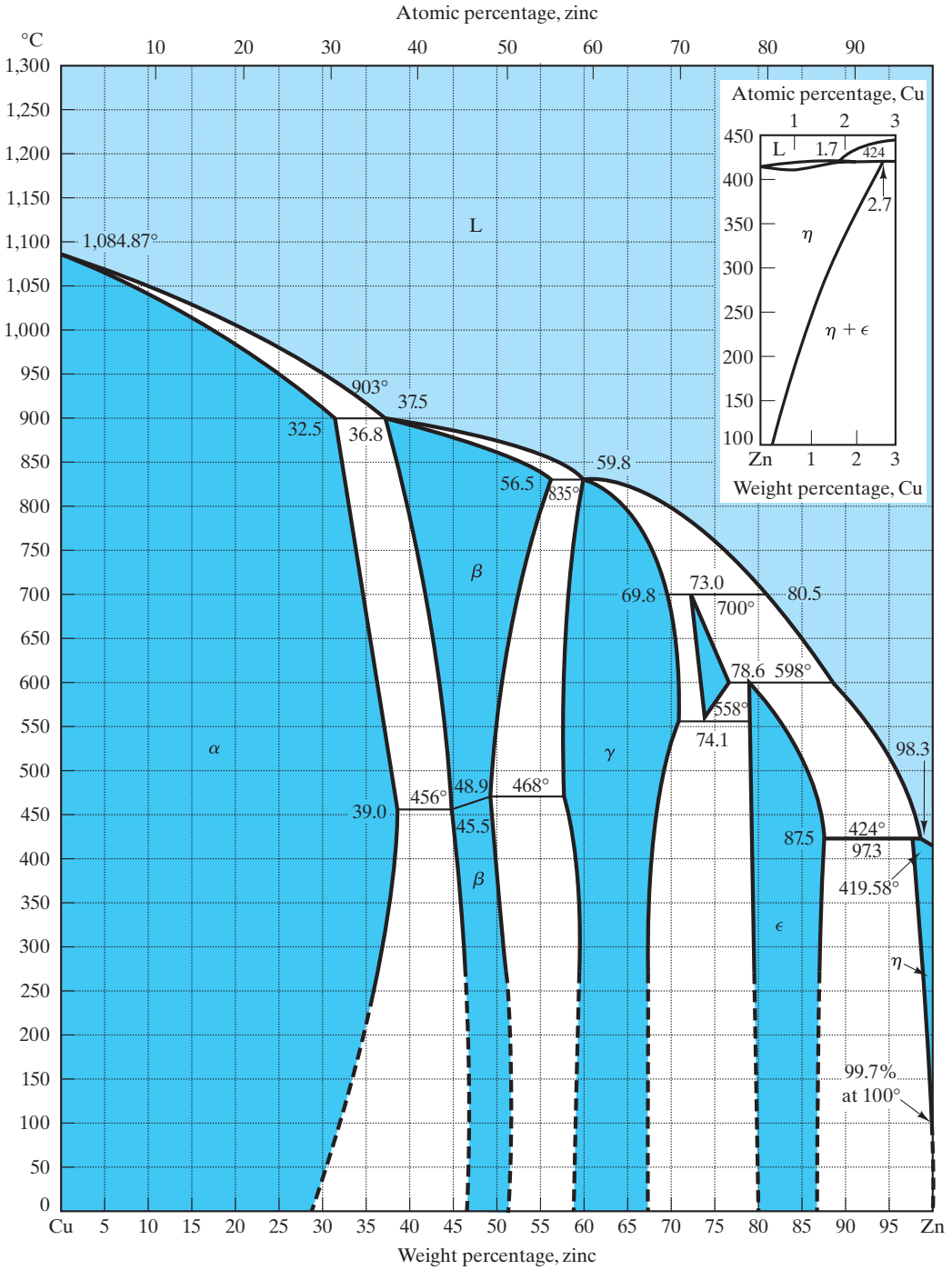

FIGURE 9.28 Cu–Zn *phase diagram. (After* Metals Handbook, *8th ed., Vol. 8:* Metallography, Structures, and Phase Diagrams, *American Society for Metals, Metals Park, OH, 1973, and* Binary Alloy Phase Diagrams, *Vol. 1, T. B. Massalski, Ed., American Society for Metals, Metals Park, OH, 1986.)*

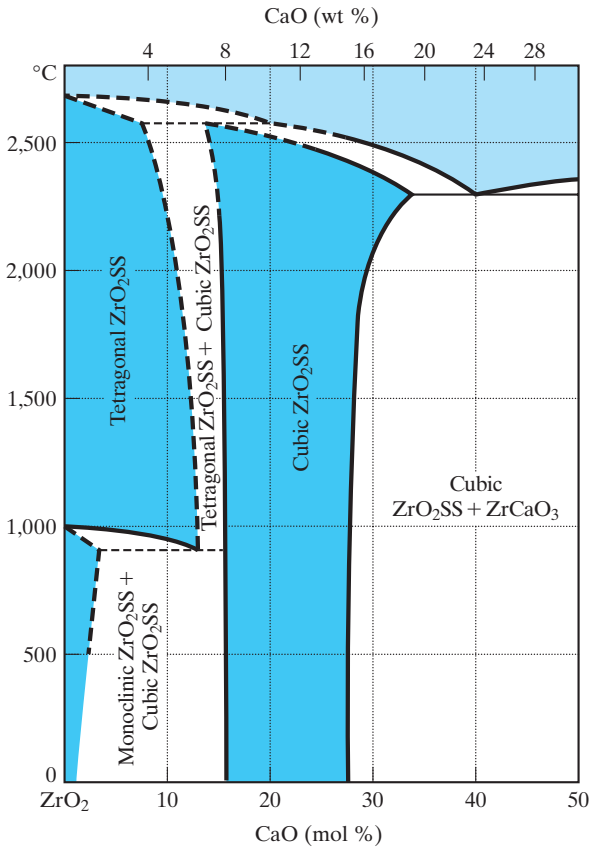

FIGURE 9.29 $CaO–ZrO_2$ *phase diagram. The dashed lines represent tentative results. (After* Phase Diagrams for Ceramists, *Vol. 1, American Ceramic Society, Columbus, OH, 1964.) (Reprinted with permission of The American Ceramic Society (www .ceramics.org). All rights reserved.)*

SOLUTION

A 50:50 combination of A and A_2B will produce an overall composition midway between A and A_2B. The cooling path is illustrated as follows:

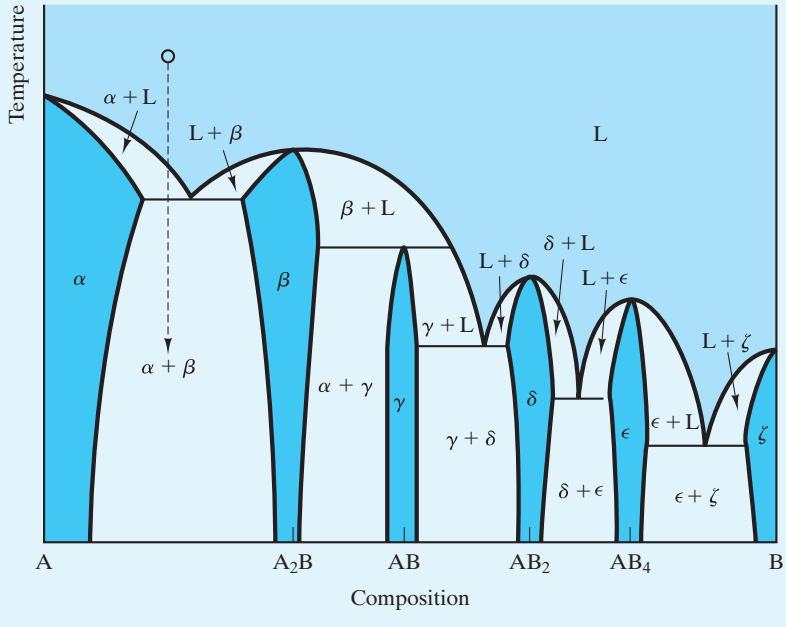

The first solid to precipitate from the liquid is the A-rich solid solution α. At the A–A_2B eutectic temperature, complete solidification occurs, giving a two-phase microstructure of solid solutions α and β.

PRACTICE PROBLEM 9.2

Qualitatively describe the microstructural development that will occur upon slow cooling of a melt of an alloy of equal parts of A_2B and AB.

9.3 The Lever Rule

In Section 9.2, we surveyed the use of phase diagrams to determine the phases present at equilibrium in a given system and their corresponding microstructure. The tie line (e.g., Figure 9.6) gives the composition of each phase in a two-phase region. We now extend this analysis to determine the amount of each phase in the two-phase region. We should first note that, for single-phase regions, the analysis is trivial. By definition, the microstructure is 100% of the single phase. In the two-phase regions, the analysis is not trivial, but is, nonetheless, simple.

The relative amounts of the two phases in a microstructure are easily calculated from a mass balance. Let us consider again the case of the binary diagram for complete solid solution. The diagram shown in Figure 9.30 is equivalent to that shown in Figure 9.6 and, again, shows a tie line that gives the composition of the two phases associated with a state point in the L + SS region. In addition, the compositions of each phase and of the overall system are indicated. An overall **mass balance** requires that the sum of the two phases equal the total system. Assuming a total mass of 100 g gives an expression

$$m_L + m_{SS} = 100\ \text{g}. \tag{9.6}$$

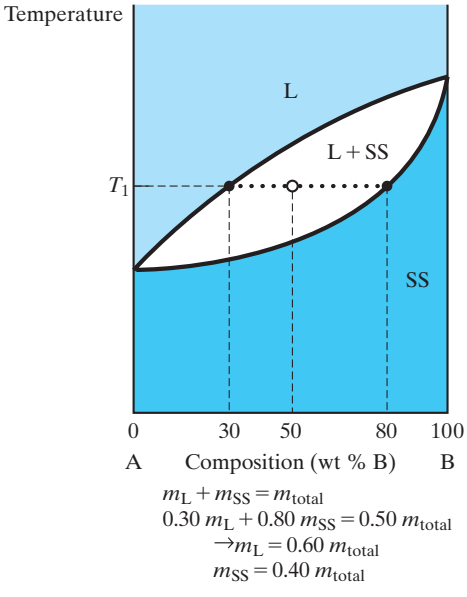

FIGURE 9.30 *A more quantitative treatment of the tie line introduced in Figure 9.6 allows the amount of each phase (*L *and* SS*) to be calculated by means of a mass balance (Equations 9.6 and 9.7).*

We can also compute an independent mass balance on either of the two components. For example, the amount of B in the liquid phase plus that in solid solution must equal the total amount of B in the overall composition. Noting in Figure 9.6 that (for temperature, T_1) L contains 30% B, SS 80% B, and the overall system 50% B, we can write

$$0.30\, m_{\mathrm{L}} + 0.80\, m_{\mathrm{SS}} = 0.50\,(100\mathrm{g}) = 50\ \mathrm{g}. \tag{9.7}$$

Equations 9.6 and 9.7 are two equations with two unknowns, allowing us to solve for the amounts of each phase:

$$m_{\mathrm{L}} = 60\ \mathrm{g}$$

and

$$m_{\mathrm{SS}} = 40\ \mathrm{g}.$$

This material-balance calculation is convenient, but an even more streamlined version can be generated. To obtain this calculation, we can compute the mass balance in general terms. For two phases, α and β, the general mass balance will be

$$x_\alpha m_\alpha + x_\beta m_\beta = x(m_\alpha + m_\beta), \tag{9.8}$$

where x_α and x_β are the compositions of the two phases and x is the overall composition. This expression can be rearranged to give the relative amount of each phase in terms of compositions:

$$\frac{m_\alpha}{m_\alpha + m_\beta} = \frac{x_\beta - x}{x_\beta - x_\alpha} \tag{9.9}$$

and

$$\frac{m_\beta}{m_\alpha + m_\beta} = \frac{x - x_\alpha}{x_\beta - x_\alpha}. \tag{9.10}$$

Together, Equations 9.9 and 9.10 constitute the **lever rule**. This mechanical analogy to the mass-balance calculation is illustrated in Figure 9.31. Its utility is due largely to the fact that it can be visualized so easily in terms of the phase diagram. The overall composition corresponds to the fulcrum of a lever with length corresponding to the tie line. The mass of each phase is suspended from the end of the lever corresponding to its composition. The relative amount of phase α is directly proportional to the length of the "opposite lever arm" ($= x_\beta - x$). It is this relationship that allows the relative amounts of phases to be determined by a simple visual inspection. With this final quantitative tool in hand, we can now proceed to the step-by-step analysis of microstructural development.

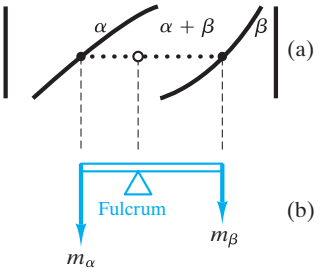

FIGURE 9.31 *The lever rule is a mechanical analogy to the mass-balance calculation. The (a) tie line in the two-phase region is analogous to (b) a lever balanced on a fulcrum.*

EXAMPLE 9.3

The temperature of 1 kg of the alloy shown in Figure 9.30 is lowered slowly until the liquid-solution composition is 18 wt % B and the solid-solution composition is 66 wt % B. Calculate the amount of each phase.

SOLUTION

Using Equations 9.9 and 9.10, we obtain

$$m_L = \frac{x_{SS} - x}{x_{SS} - x_L}(1\text{ kg}) = \frac{66 - 50}{66 - 18}(1\text{ kg})$$
$$= 0.333\text{ kg} = 333\text{ g}$$

and

$$m_{SS} = \frac{x - x_L}{x_{SS} - x_L}(1\text{ kg}) = \frac{50 - 18}{66 - 18}(1\text{ kg})$$
$$= 0.667\text{ kg} = 667\text{ g}.$$

Note. We can also calculate m_{SS} more swiftly by simply noting that $m_{SS} = 1{,}000\text{ g} - m_L = (1{,}000 - 333)\text{ g} = 667\text{ g}$. However, we shall continue to use both Equations 9.9 and 9.10 in the example problems in this chapter for the sake of practice and as a cross-check.

EXAMPLE 9.4

For 1 kg of eutectoid steel at room temperature, calculate the amount of each phase (α and Fe_3C) present.

SOLUTION

Using Equations 9.9 and 9.10 and Figure 9.19, we have

$$m_\alpha = \frac{x_{Fe_3C} - x}{x_{Fe_3C} - x_\alpha}(1\text{ kg}) = \frac{6.69 - 0.77}{6.69 - 0}(1\text{ kg})$$
$$= 0.885\text{ kg} = 885\text{ g}$$

and

$$m_{Fe_3C} = \frac{x - x_\alpha}{x_{Fe_3C} - x_\alpha}(1\text{ kg}) = \frac{0.77 - 0}{6.69 - 0}(1\text{ kg})$$
$$= 0.115\text{ kg} = 115\text{ g}.$$

EXAMPLE 9.5

A partially stabilized zirconia is composed of 4 wt % CaO. This product contains some monoclinic phase together with the cubic phase, which is the basis of fully stabilized zirconia. Estimate the mole percent of each phase present at room temperature.

SOLUTION

Noting that 4 wt % CaO = 8 mol % CaO and assuming that the solubility limits shown in Figure 9.29 do not change significantly below

500°C, we can use Equations 9.9 and 9.10:

$$\text{mol \% monoclinic} = \frac{x_{\text{cub}} - x}{x_{\text{cub}} - x_{\text{mono}}} \times 100\% = \frac{15 - 8}{15 - 2} \times 100\% = 53.8 \text{ mol \%}$$

and

$$\text{mol \% cubic} = \frac{x - x_{\text{mono}}}{x_{\text{cub}} - x_{\text{mono}}} \times 100\% = \frac{8 - 2}{15 - 2} \times 100\% = 46.2 \text{ mol \%}.$$

THE MATERIAL WORLD

Purifying Semiconductors by Zone Refining

The Feature Box in Chapter 3 gave us an appreciation of how semiconductors are produced with a high degree of structural perfection. In Chapter 13, we will see that solid-state electronics also require that semiconductors have a high degree of chemical purity. This chemical perfection is due to a special process prior to the crystal-growing step. This process is, in fact, a creative use of phase diagrams.

As seen in the following illustration, a bar of material (e.g., silicon) with a modest level of impurities is purified by the process of **zone refining**. In this technique, an induction coil produces a local molten "zone." As the coil passes along the length of the bar, the zone follows along. The molten material solidifies as soon as the induction coil moves away.

The following phase diagram illustrates that the impurity content in the liquid is substantially greater than in the solid. As a result, a single pass of the heating coil along the bar "sweeps" the impurities along with the liquid zone to one end. Multiple passes lead to substantial purification. Eventually, substantial levels of contamination will be swept to one end of the bar, which is simply sawed off and discarded. For the bulk of the bar, impurity levels in the parts per billion (ppb) range are practical and, in fact, were necessary to allow the development of solid-state electronics as we know it today.

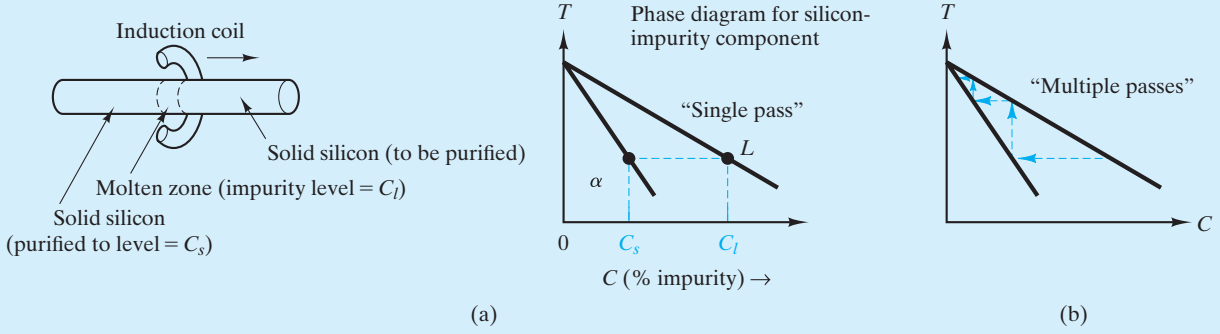

In zone refining, (a) a single pass of the molten "zone" through the bar leads to the concentration of impurities in the liquid. This is illustrated by the nature of the phase diagram. (b) Multiple passes of the molten zone increases purification of the solid.

PRACTICE PROBLEM 9.3

Suppose the alloy in Example 9.3 is reheated to a temperature at which the liquid composition is 48 wt % B and the solid-solution composition is 90 wt % B. Calculate the amount of each phase.

PRACTICE PROBLEM 9.4

In Example 9.4, we found the amount of each phase in a eutectoid steel at room temperature. Repeat this calculation for a steel with an overall composition of 1.13 wt % C.

PRACTICE PROBLEM 9.5

In Example 9.5, the phase distribution in a partially stabilized zirconia is calculated. Repeat this calculation for a zirconia with 5 wt % CaO.

9.4 Microstructural Development During Slow Cooling

We are now in a position to follow closely the **microstructural development** in various binary systems. In all cases, we shall assume the common situation of cooling a given composition from a single-phase melt. Microstructure is developed in the process of solidification. We consider only the case of *slow* cooling; that is, equilibrium is essentially maintained at all points along the cooling path. The effect of more rapid temperature changes is the subject of Chapter 10, which deals with time-dependent microstructures developed during heat treatment.

Let us return to the simplest of binary diagrams, the case of complete solubility in both the liquid and solid phases. Figure 9.32 shows the gradual solidification of the 50% A–50% B composition treated previously (Figures 9.6, 9.8, and 9.30). The lever rule (Figure 9.31) is applied at three different temperatures in the two-phase (L + SS) region. It is important to appreciate that the appearance of the microstructures in Figure 9.32 corresponds directly with the relative position of the overall system composition along the tie line. At higher temperatures (e.g., T_1), the overall composition is near the liquid-phase boundary, and the microstructure is predominantly liquid. At lower temperatures (e.g., T_3), the overall composition is near the solid-phase boundary, and the microstructure is predominantly solid. Of course, the compositions of the liquid and solid phases change continuously during cooling through the two-phase region. At any temperature, however, the relative amounts of each phase are such that the overall composition is 50% A and 50% B, which is a direct manifestation of the lever rule as defined by the mass balance of Equation 9.8.

The understanding of microstructural development in the binary eutectic is greatly aided by the lever rule. The case for the eutectic composition itself is straightforward and was illustrated previously (Figures 9.12 and 9.15). Figure 9.33 repeats those cases in slightly greater detail. An additional comment is that the composition of each solid-solution phase (α and β) and their relative amounts

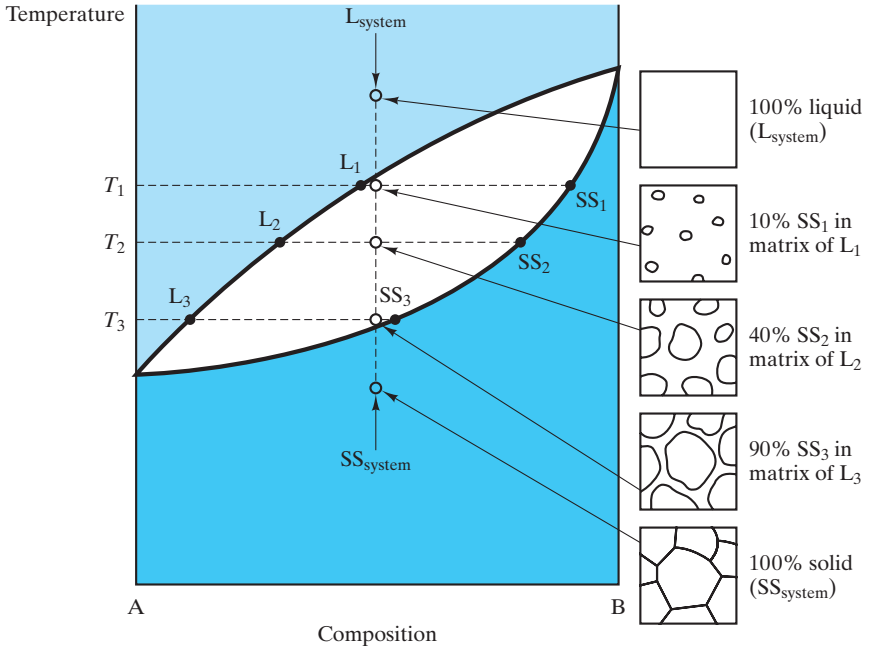

FIGURE 9.32 *Microstructural development during the slow cooling of a* 50% A–50% B *composition in a phase diagram with complete solid solution. At each temperature, the amounts of the phases in the microstructure correspond to a lever-rule calculation. The microstructure at T_2 corresponds to the calculation in Figure 9.30.*

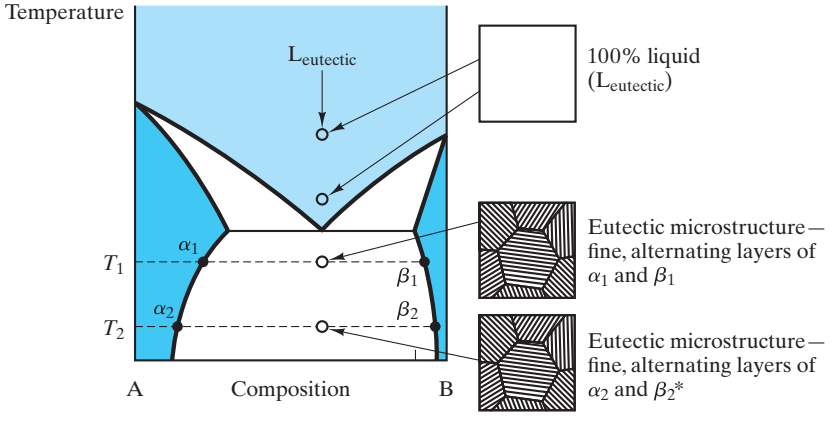

*The only differences between this structure and the T_1 microstructure are the phase compositions and the relative amounts of each phase. For example, the amount of β will be proportional to

$$\frac{x_{eutectic} - x_\alpha}{x_\beta - x_\alpha}.$$

FIGURE 9.33 *Microstructural development during the slow cooling of a eutectic composition.*

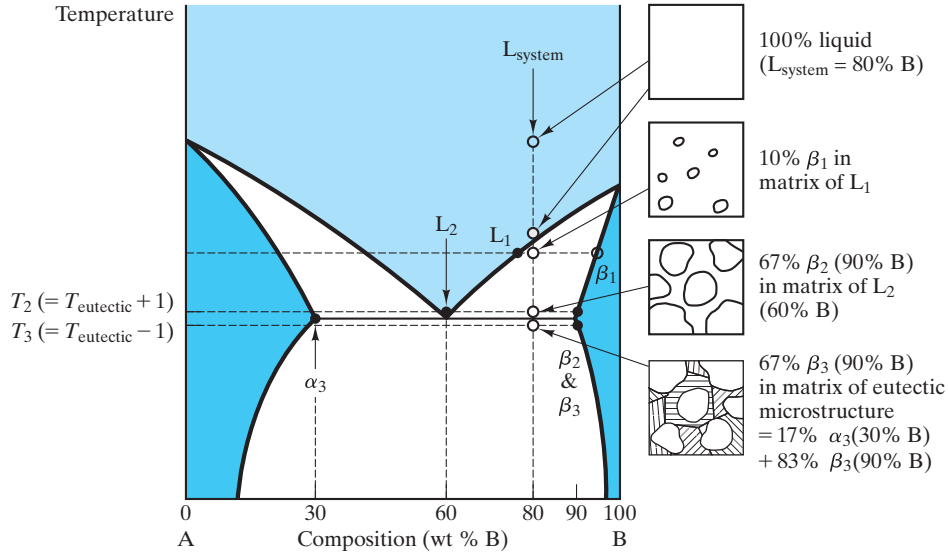

FIGURE 9.34 *Microstructural development during the slow cooling of a hypereutectic composition.*

will change slightly with temperature below the eutectic temperature. The microstructural effect (corresponding to this compositional adjustment due to solid-state diffusion) is generally minor.

Microstructural development for a noneutectic composition is more complex. Figure 9.34 illustrates the microstructural development for a **hypereutectic composition** (composition greater than that of the eutectic). The gradual growth of β crystals above the eutectic temperature is comparable to the process found in Figure 9.32 for the complete solid-solution diagram. The one difference is that, in Figure 9.34, the crystallite growth stops at the eutectic temperature with only 67% of the microstructure solidified. Final solidification occurs when the remaining liquid (with the eutectic composition) transforms suddenly to the eutectic microstructure upon cooling through the eutectic temperature. In a sense, the 33% of the microstructure that is liquid just above the eutectic temperature undergoes the eutectic reaction illustrated in Figure 9.33. A lever-rule calculation just below the eutectic temperature (T_3 in Figure 9.34) indicates correctly that the microstructure is 17% α_3 and 83% β_3. However, following the entire cooling path has indicated that the β phase is present in two forms. The large grains produced during the slow cooling through the two-phase (L + β) region are termed **proeutectic** β; that is, they appear "before the eutectic." The finer β in the lamellar eutectic is appropriately termed *eutectic* β.

Figure 9.35 shows a similar situation that develops for a **hypoeutectic composition** (composition less than that of the eutectic). This case is analogous to that for the hypereutectic composition. In Figure 9.35, we see the development of large grains of proeutectic α along with the eutectic microstructure of α and β layers. Two other types of microstructural development are illustrated in Figure 9.36. For an overall composition of 10% B, the situation

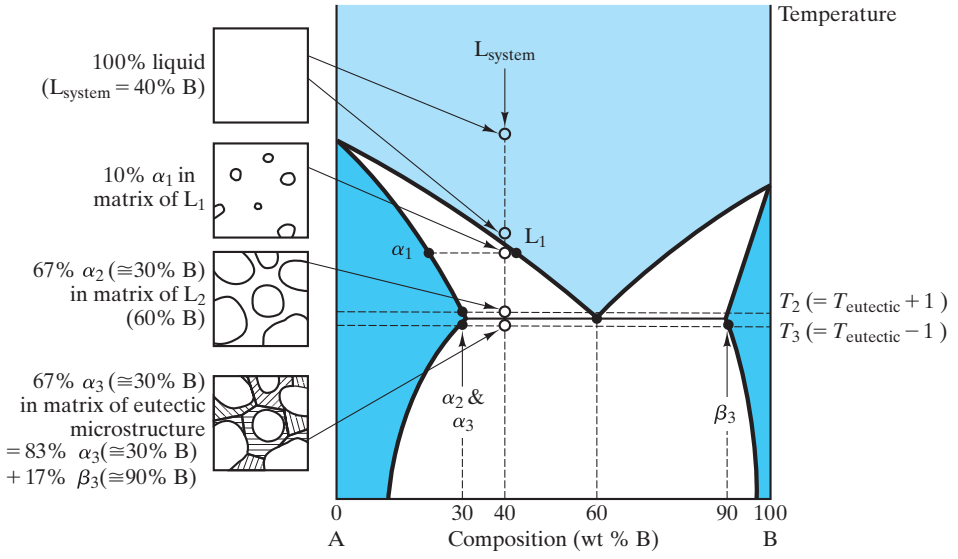

FIGURE 9.35 *Microstructural development during the slow cooling of a hypoeutectic composition.*

is quite similar to that for the complete solid-solution binary in Figure 9.32. The solidification leads to a single-phase solid solution that remains stable upon cooling to low temperatures. The 20% B composition behaves in a similar fashion except that, upon cooling, the α phase becomes saturated with B atoms. Further cooling leads to precipitation of a small amount of β phase. In Figure 9.36(b), this precipitation is shown occurring along grain boundaries. In some systems, the second phase precipitates within grains. For a given

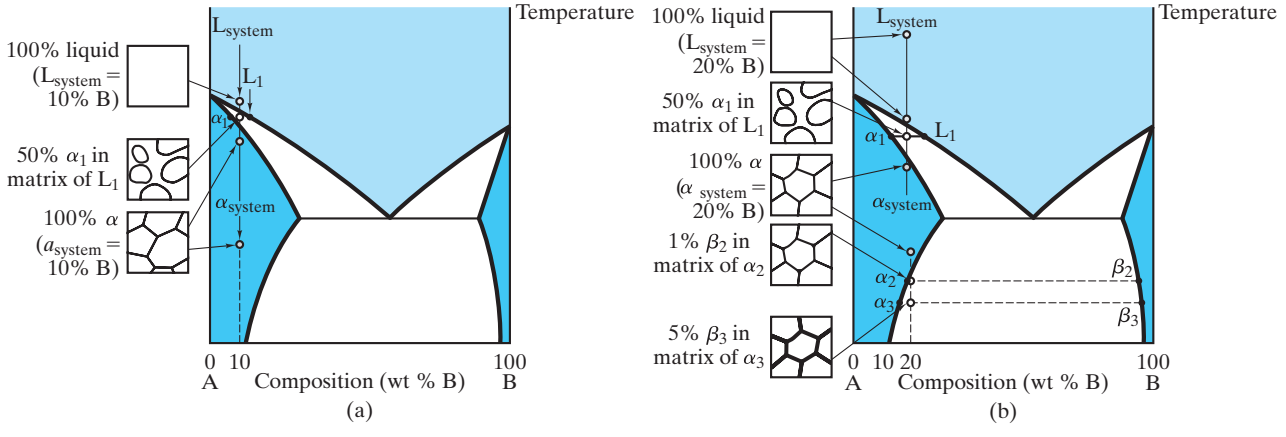

FIGURE 9.36 *Microstructural development for two compositions that avoid the eutectic reaction.*

system, the morphology of the second phase can be a sensitive function of the rate of cooling. In Section 10.4, we shall encounter such a case for the Al–Cu system, in which precipitation hardening is an important example of heat treatment.

With the variety of cases encountered in this section, we are now in a position to treat any composition in any of the binary systems presented in this chapter, including the general diagrams represented by Figure 9.25(b).

The cooling path for a **white cast iron** (see also Chapter 11) is shown in Figure 9.37. The schematic microstructure can be compared with a micrograph in Figure 11.1(a). The eutectoid reaction to produce pearlite is shown in Figure 9.38. This composition (0.77 wt % C) is close to that for a 1080 plain-carbon steel (see Table 11.1). Many phase diagrams for the Fe–Fe_3C system give the eutectoid composition rounded off to 0.8 wt % C. As a practical matter, any composition near 0.77 wt % C will give a microstructure

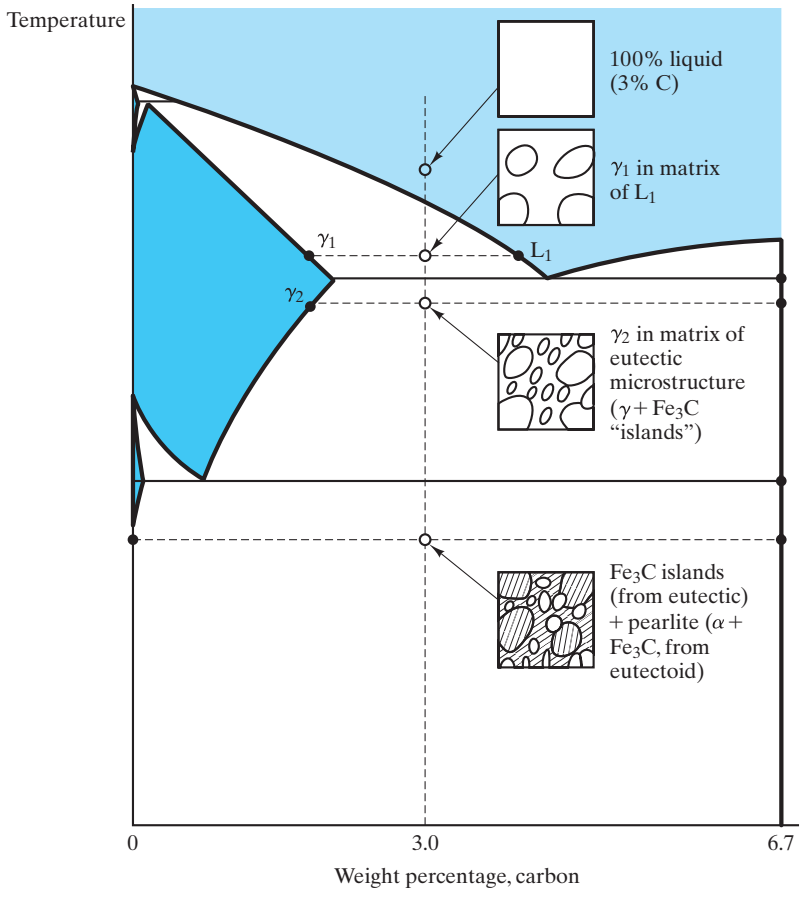

FIGURE 9.37 *Microstructural development for white cast iron (of composition* 3.0 *wt % C) shown with the aid of the* Fe−Fe_3C *phase diagram. The resulting (low-temperature) sketch can be compared with a micrograph in Figure 11.1(a).*

EXAMPLE 9.6

Figure 9.34 shows the microstructural development for an 80 wt% B alloy. Consider instead 1 kg of a 70 wt % B alloy.

(a) Calculate the amount of β phase at T_3.

(b) Calculate what weight fraction of this β phase at T_3 is proeutectic.

SOLUTION

(a) Using Equation 9.10 gives us

$$m_{\beta,T_3} = \frac{x - x_\alpha}{x_\beta - x_\alpha}(1\text{ kg}) = \frac{70 - 30}{90 - 30}(1\text{ kg})$$

$$= 0.667\text{ kg} = 667\text{ g}.$$

that is predominantly eutectoid. The actual pearlite microstructure is shown in the micrograph of Figure 9.2. A **hypereutectoid composition** (composition greater than the eutectoid composition of 0.77 wt % C) is treated in Figure 9.39. This case is similar in many ways to the hypereutectic path shown

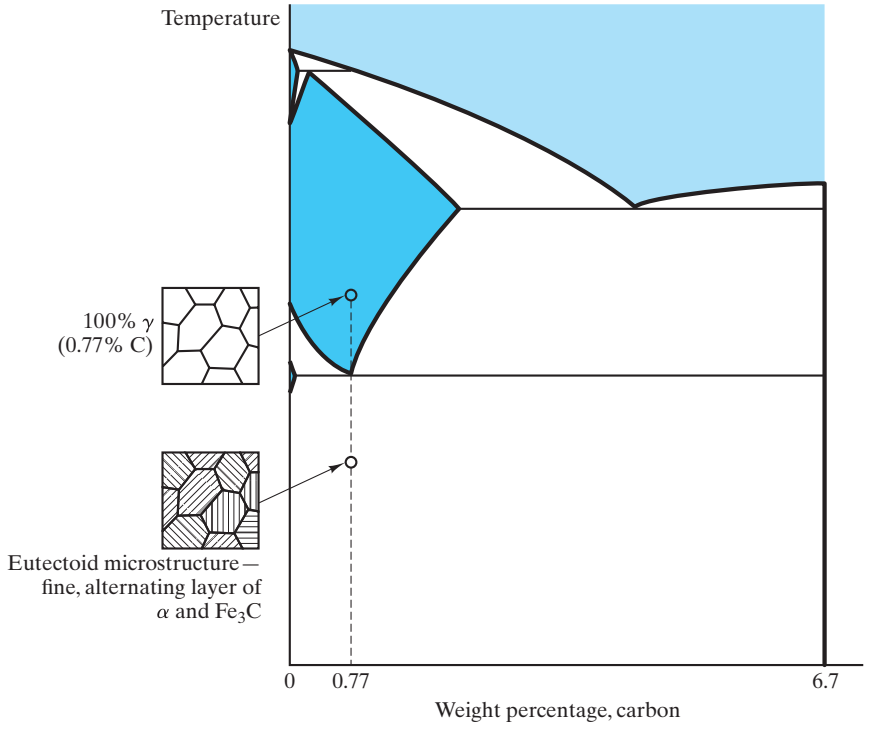

FIGURE 9.38 *Microstructural development for eutectoid steel (of composition* 0.77 *wt % C). The resulting (low-temperature) sketch can be compared with the micrograph in Figure 9.2.*

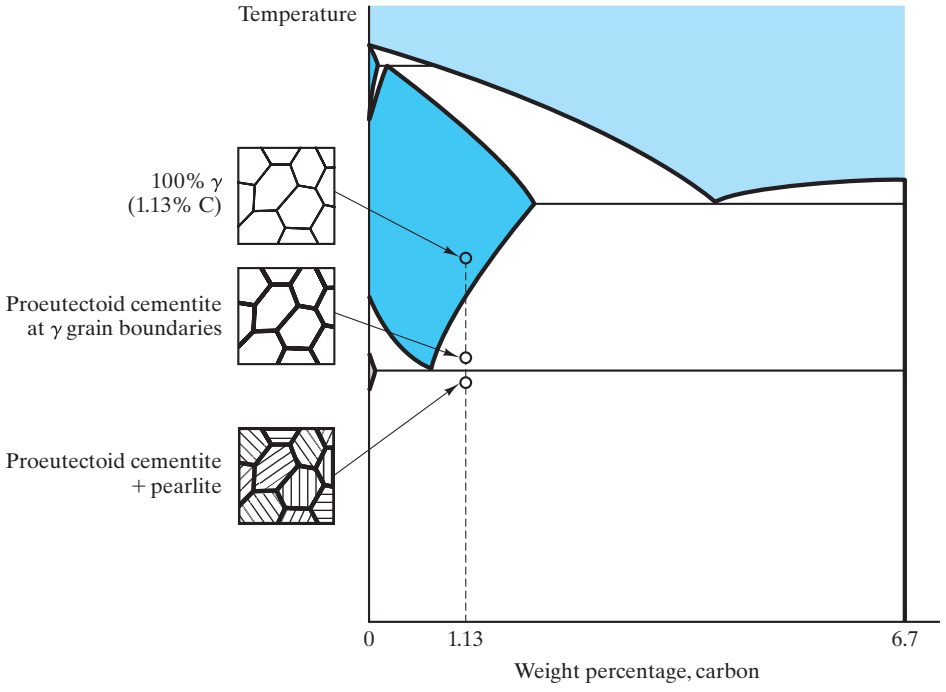

FIGURE 9.39 *Microstructural development for a slowly cooled hypereutectoid steel (of composition* 1.13 *wt %* C*).*

in Figure 9.34. A fundamental difference is that the **proeutectoid** cementite (Fe_3C) is the matrix in the final microstructure, whereas the proeutectic phase in Figure 9.34 was the isolated phase. The formation of the proeutectoid matrix occurs because the precipitation of proeutectoid cementite is a

(b) The proeutectic β was that which was present in the microstructure at T_2:

$$m_{\beta,T_2} = \frac{x - x_L}{x_\beta - x_L}(1\text{ kg}) = \frac{70 - 60}{90 - 60}(1\text{ kg})$$

$$= 0.333\text{ kg} = 333\text{ g}.$$

This portion of the microstructure is retained upon cooling through the eutectic temperature, giving

$$\text{fraction proeutectic} = \frac{\text{proeutectic }\beta}{\text{total }\beta}$$

$$= \frac{333\text{ g}}{667\text{ g}} = 0.50.$$

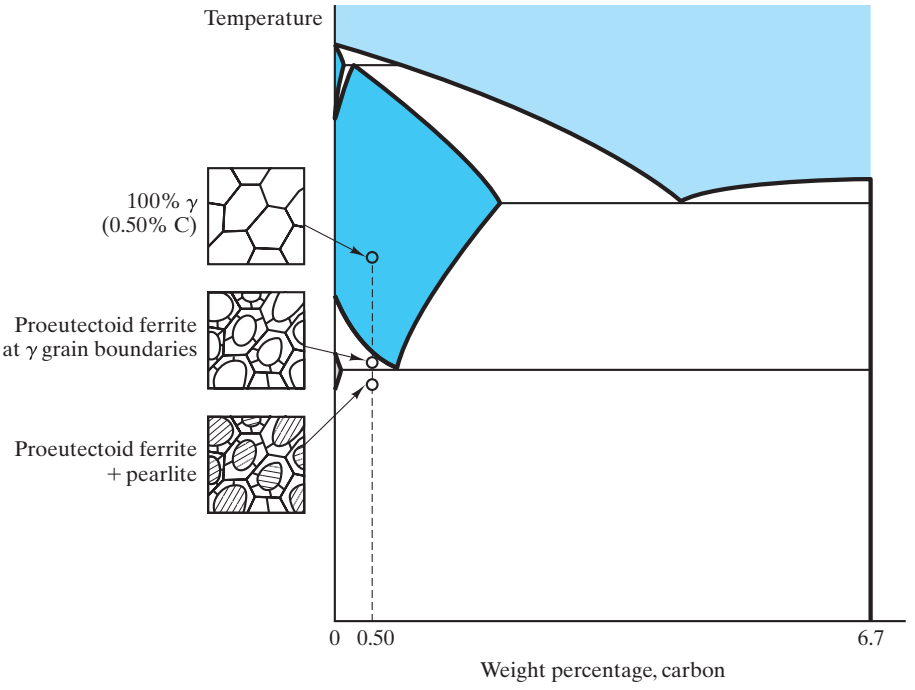

FIGURE 9.40 *Microstructural development for a slowly cooled hypoeutectoid steel (of composition* 0.50 *wt* % C*).*

solid-state transformation and is favored at grain boundaries. Figure 9.40 illustrates the development of microstructure for a **hypoeutectoid composition** (less than 0.77 wt % C).

The Fe–C system (Figure 9.20) provides an illustration of the development of the microstructure of **gray cast iron** (Figure 9.41). This sketch can be compared with the micrograph in Figure 11.1(b).

EXAMPLE 9.7

For 1 kg of 0.5 wt % C steel, calculate the amount of proeutectoid α at the grain boundaries.

SOLUTION

Using Figure 9.40 for illustration and Figure 9.19 for calculation, we essentially need to calculate the equilibrium amount of α at 728°C (i.e., 1 degree above the eutectoid temperature). Using Equation 9.9, we have

$$m_\alpha = \frac{x_\gamma - x}{x_\gamma - x_\alpha}(1\text{ kg}) = \frac{0.77 - 0.50}{0.77 - 0.02}(1\text{ kg})$$
$$= 0.360\text{ kg} = 360\text{ g}.$$

Note. You might have noticed that this calculation near the eutectoid composition used a value of x_α representative of the maximum solubility of carbon in α-Fe (0.02 wt %). At room temperature (see Example 9.4), this solubility goes to nearly zero.

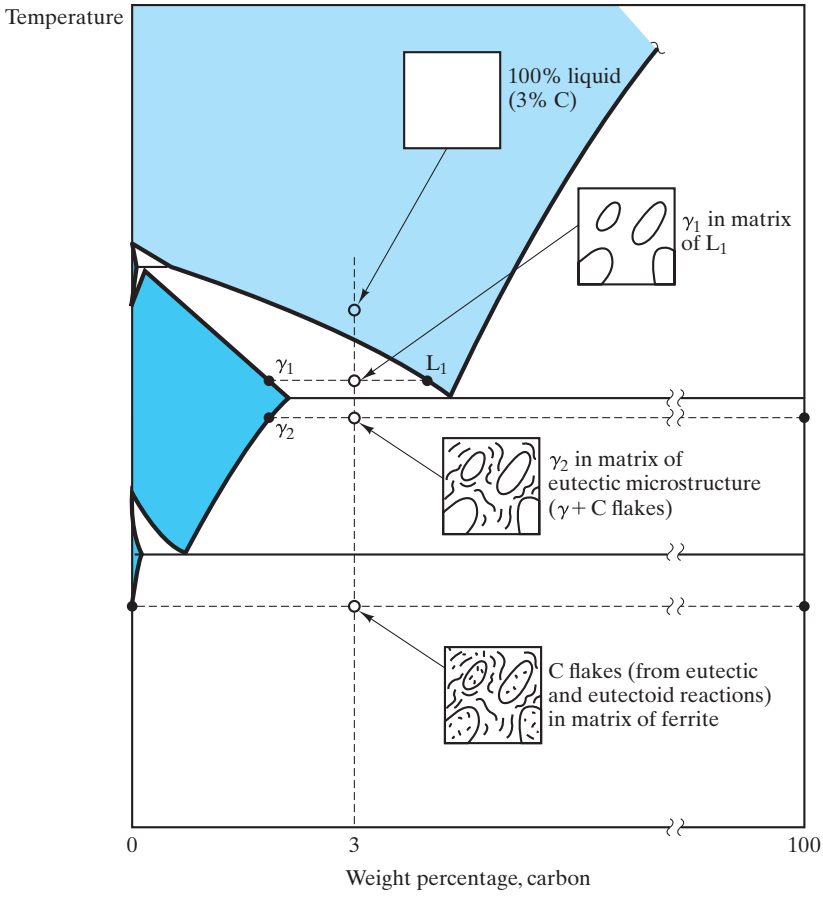

FIGURE 9.41 *Microstructural development for gray cast iron (of composition* 3.0 *wt % C) shown on the* Fe–C *phase diagram. The resulting low-temperature sketch can be compared with the micrograph in Figure 11.1(b). A dramatic difference is that, in the actual microstructure, a substantial amount of metastable pearlite was formed at the eutectoid temperature. It is also interesting to compare this sketch with that for white cast iron in Figure 9.37. The small amount of silicon added to promote graphite precipitation is not shown in this two-component diagram.*

EXAMPLE 9.8

For 1 kg of 3 wt % C gray iron, calculate the amount of graphite flakes present in the microstructure **(a)** at 1,153°C and **(b)** at room temperature.

SOLUTION

(a) Using Figures 9.20 and 9.41, we note that 1,153°C is just below the eutectic temperature. Using Equation 9.10 gives us

$$m_C = \frac{x - x_\gamma}{x_C - x_\gamma}(1\text{ kg}) = \frac{3.00 - 2.08}{100 - 2.08}(1\text{ kg})$$
$$= 0.00940\text{ kg} = 9.40\text{ g}.$$

(b) At room temperature, we obtain

$$m_C = \frac{x - x_\alpha}{x_C - x_\alpha}(1\text{ kg}) = \frac{3.00 - 0}{100 - 0}(1\text{ kg})$$
$$= 0.030\text{ kg} = 30.0\text{ g}.$$

Note. This calculation follows the ideal system of Figure 9.41 and ignores the possibility of any metastable pearlite being formed.

EXAMPLE 9.9

Consider 1 kg of an aluminum casting alloy with 10 wt % silicon.

(a) Upon cooling, at what temperature would the first solid appear?
(b) What is the first solid phase, and what is its composition?
(c) At what temperature will the alloy completely solidify?
(d) How much proeutectic phase will be found in the microstructure?
(e) How is the silicon distributed in the microstructure at 576°C?

SOLUTION

We follow this microstructural development with the aid of Figure 9.13.

(a) For this composition, the liquidus is at ~595°C.
(b) It is solid solution α with a composition of ~1 wt % Si.
(c) At the eutectic temperature, 577°C.
(d) Practically all of the proeutectic α will have developed by 578°C. Using Equation 9.9, we obtain

$$m_\alpha = \frac{x_L - x}{x_L - x_\alpha}(1\text{ kg}) = \frac{12.6 - 10}{12.6 - 1.6}(1\text{ kg})$$
$$= 0.236\text{ kg} = 236\text{ g}.$$

(e) At 576°C, the overall microstructure is $\alpha + \beta$. The amounts of each are

$$m_\alpha = \frac{x_\beta - x}{x_\beta - x_\alpha}(1\text{ kg}) = \frac{100 - 10}{100 - 1.6}(1\text{ kg})$$
$$= 0.915\text{ kg} = 915\text{ g}$$

and

$$m_\beta = \frac{x - x_\alpha}{x_\beta - x_\alpha}(1\text{ kg}) = \frac{10 - 1.6}{100 - 1.6}(1\text{ kg})$$
$$= 0.085\text{ kg} = 85\text{ g}.$$

However, we found in (d) that 236 g of the α is in the form of relatively large grains of proeutectic phase, giving

$$\alpha_{\text{eutectic}} = \alpha_{\text{total}} - \alpha_{\text{proeutectic}}$$
$$= 915\text{ g} - 236\text{ g} = 679\text{ g}.$$

The silicon distribution is then given by multiplying its weight fraction in each microstructural region by the amount of that region:

$$\text{Si in proeutectic } \alpha = (0.016)(236\text{ g}) = 3.8\text{ g},$$
$$\text{Si in eutectic } \alpha = (0.016)(679\text{ g}) = 10.9\text{ g},$$

and

$$\text{Si in eutectic } \beta = (1.000)(85\text{ g}) = 85.0\text{ g}.$$

Finally, note that the total mass of silicon in the three regions sums to 99.7 g rather than 100.0 g (= 10 wt % of the total alloy) due to round-off errors.

EXAMPLE 9.10

The solubility of copper in aluminum drops to nearly zero at 100°C. What is the maximum amount of θ phase that will precipitate out in a 4.5 wt % copper alloy quenched and aged at 100°C? Express your answer in weight percent.

SOLUTION

As indicated in Figure 9.27, the solubility limit of the θ phase is essentially unchanging with temperature below ~400°C and is near a

composition of 53 wt % copper. Using Equation 9.10 gives us

$$\text{wt \% } \theta = \frac{x - x_\kappa}{x_\theta - x_\kappa} \times 100\% = \frac{4.5 - 0}{53 - 0} \times 100\%$$
$$= 8.49\%.$$

EXAMPLE 9.11

In Example 9.1, we considered a 50:50 Pb–Sn solder.

(a) For a temperature of 200°C, determine (i) the phases present, (ii) their compositions, and (iii) their relative amounts (expressed in weight percent).

(b) Repeat part (a) for 100°C.

SOLUTION

(a) Using Figure 9.16, we find the following results at 200°C:

i. The phases are α and liquid.

ii. The composition of α is ~18 wt % Sn and of L is ~54 wt % Sn.

iii. Using Equations 9.9 and 9.10, we have

$$\text{wt \% } \alpha = \frac{x_L - x}{x_L - x_\alpha} \times 100\% = \frac{54 - 50}{54 - 18} \times 100\%$$
$$= 11.1\%$$

and

$$\text{wt \% L} = \frac{x - x_\alpha}{x_L - x_\alpha} \times 100\% = \frac{50 - 18}{54 - 18} \times 100\%$$
$$= 88.9\%.$$

(b) Similarly, at 100°C, we obtain

i. α and β.

ii. α is ~5 wt % Sn and β is ~99 wt % Sn.

iii. $$\text{wt \% } \alpha = \frac{x_\beta - x}{x_\beta - x_\alpha} \times 100\% = \frac{99 - 50}{99 - 5} \times 100\% = 52.1\%$$

and

$$\text{wt \% } \beta = \frac{x - x_\alpha}{x_\beta - x_\alpha} \times 100\% = \frac{50 - 5}{99 - 5} \times 100\% = 47.9\%.$$

EXAMPLE 9.12

A fireclay refractory ceramic can be made by heating the raw material kaolinite, $Al_2(Si_2O_5)(OH)_4$, thus driving off the waters of hydration. Determine the phases present, their compositions, and their amounts for the resulting microstructure (below the eutectic temperature).

SOLUTION

A modest rearrangement of the kaolinite formula helps to clarify the production of this ceramic product:

$$Al_2(Si_2O_5)(OH)_4 = Al_2O_3 \cdot 2SiO_2 \cdot 2H_2O.$$

The firing operation yields

$$Al_2O_3 \cdot 2SiO_2 \cdot 2H_2O \xrightarrow{\text{heat}} Al_2O_3 \cdot 2SiO_2 + 2H_2O \uparrow.$$

The remaining solid, then, has an overall composition of

$$\text{mol \% } Al_2O_3 = \frac{\text{mol } Al_2O_3}{\text{mol } Al_2O_3 + \text{mol } SiO_2} \times 100\%$$

$$= \frac{1}{1+2} \times 100\% = 33.3\%.$$

Using Figure 9.23, we see that the overall composition falls in the SiO_2 + mullite two-phase region below the eutectic temperature. The SiO_2 composition is 0 mol % Al_2O_3 (i.e., 100% SiO_2). The composition of mullite is 60 mol % Al_2O_3.

Using Equations 9.9 and 9.10 yields

$$\text{mol \% } SiO_2 = \frac{x_{\text{mullite}} - x}{x_{\text{mullite}} - x_{SiO_2}} \times 100\% = \frac{60 - 33.3}{60 - 0} \times 100\%$$

$$= 44.5 \text{ mol \%}$$

and

$$\text{mol \% mullite} = \frac{x - x_{SiO_2}}{x_{\text{mullite}} - x_{SiO_2}} \times 100\% = \frac{33.3 - 0}{60 - 0} \times 100\%$$

$$= 55.5 \text{ mol \%}.$$

Note. Because the Al_2O_3–SiO_2 phase diagram is presented in mole percent, we have made our calculations in a consistent system. It would be a minor task to convert results to weight percent using data from Appendix 1.

PRACTICE PROBLEM 9.6

In Example 9.6, we calculate microstructural information about the β phase for the 70 wt % B alloy in Figure 9.34. In a similar way, calculate **(a)** the amount of α phase at T_3 for 1 kg of a 50 wt % B alloy and **(b)** the weight fraction of this α phase at T_3, which is proeutectic. (See also Figure 9.35.)

PRACTICE PROBLEM 9.7

Calculate the amount of proeutectoid cementite at the grain boundaries in 1 kg of the 1.13 wt % C hypereutectoid steel illustrated in Figure 9.39. (See Example 9.7.)

PRACTICE PROBLEM 9.8

In Example 9.8, the amount of carbon in 1 kg of a 3 wt % C gray iron is calculated at two temperatures. Plot the amount as a function of temperature over the entire temperature range of 1,135°C to room temperature.

PRACTICE PROBLEM 9.9

In Example 9.9, we monitor the microstructural development for 1 kg of a 10 wt % Si–90 wt % Al alloy. Repeat this problem for a 20 wt % Si–80 wt % Al alloy.

PRACTICE PROBLEM 9.10

In Example 9.10, we calculate the weight percent of θ phase at room temperature in a 95.5 Al–4.5 Cu alloy. Plot the weight percent of θ (as a function of temperature) that would occur upon slow cooling over a temperature range of 548°C to room temperature.

PRACTICE PROBLEM 9.11

Calculate microstructures for **(a)** a 40:60 Pb–Sn solder and **(b)** a 60:40 Pb–Sn solder at 200°C and 100°C. (See Example 9.11.)

PRACTICE PROBLEM 9.12

In the note at the end of Example 9.12, the point is made that the results can be easily converted to weight percent. Make these conversions.

Summary

The development of microstructure during slow cooling of materials from the liquid state can be analyzed using phase diagrams. These "maps" identify the amounts and compositions of phases that are stable at given temperatures. Phase diagrams can be thought of as visual displays of the Gibbs phase rule. In this chapter, we restricted our discussion to binary diagrams, which represent phases present at various temperatures and compositions (with pressure fixed at 1 atm) in systems with two components; the components can be elements or compounds.

Several types of binary diagrams are commonly encountered. For very similar components, complete solid solution can occur in the solid state as well as in the liquid state. In the two-phase (liquid solution + solid solution) region, the composition of each phase is indicated by a tie line. Many binary systems exhibit a eutectic reaction in which a

low melting point (eutectic) composition produces a fine-grained, two-phase microstructure. Such eutectic diagrams are associated with limited solid solution. The completely solid-state analogy to the eutectic reaction is the eutectoid reaction, in which a single solid phase transforms upon cooling to a fine-grained microstructure of two other solid phases. The peritectic reaction represents the incongruent melting of a solid compound. Upon melting, the compound transforms to a liquid and another solid, each of composition different from the original compound. Many binary diagrams include various intermediate compounds, leading to a relatively complex appearance. However, such general binary diagrams can always be reduced to a simple binary diagram associated with the overall composition of interest.

The tie line that identifies the compositions of the phases in a two-phase region can also be used to calculate the amount of each phase. This calculation is done using the lever rule, in which the tie line is treated as a lever with its fulcrum located at the overall composition. The amounts of the two phases are such that they "balance the lever." The lever rule is, of course, a mechanical analog, but it follows directly from a mass balance for the two-phase system. The lever rule can be used to follow microstructural development as an overall composition is slowly cooled from the melt, which is especially helpful in understanding the microstructure that results in a composition near a eutectic composition. Several binary diagrams of importance to the metals and ceramics industries were given in this chapter. Special emphasis was given to the $Fe-Fe_3C$ system, which provides the major scientific basis for the iron and steel industries.

Key Terms

austenite (270)
binary diagram (261)
complete solid solution (262)
component (258)
congruent melting (272)
degrees of freedom (259)
eutectic composition (266)
eutectic diagram (266)
eutectic reaction (270)
eutectic temperature (266)
eutectoid diagram (270)
general diagram (275)
Gibbs phase rule (259)
gray cast iron (289)
hypereutectic composition (287)
hypereutectoid composition (288)
hypoeutectic composition (287)
hypoeutectoid composition (289)
incongruent melting (272)
intermediate compound (275)
invariant point (263)
lever rule (282)
liquidus (262)
mass balance (281)
metastable (271)
microstructural development (285)
peritectic diagram (272)
peritectic reaction (272)
phase (258)
phase diagram (261)
phase field (262)
proeutectic (287)
proeutectoid (288)
solidus (262)
state (259)
state point (262)
state variables (259)
tie line (263)
white cast iron (288)
zone refining (284)

References

ASM Handbook, Vol. 3: *Alloy Phase Diagrams,* ASM International, Materials Park, OH, 1992.

Binary Alloy Phase Diagrams, 2nd ed., Vols. 1–3, T. B. Massalski, et al., Eds., ASM International, Materials Park, OH, 1990. The result of a cooperative program between ASM International and the National Institute of Standards and Technology for the critical review of 4,700 phase-diagram systems.

Phase Equilibria Diagrams, Vols. 1–14, American Ceramic Society, Westerville, OH, 1964–2005.